Critical Reviews in Solid State and Materials Sciences, 30:1–31, 2005

ISSN: 1040-8436 print
DOI: 10.1080/10408430590918341

Taylor & Francis
Taylor & Francis Group

Thin Film Deposition Methods for $CuInSe_2$ Solar Cells

Marianna Kemell,* Mikko Ritala, and Markku Leskelä
Laboratory of Inorganic Chemistry, Department of Chemistry, University of Helsinki, Helsinki, Finland

$CuInSe_2$ and its alloys with Ga and/or S are among the most promising absorber materials for thin film solar cells. $CuInSe_2$-based solar cells have shown long-term stability and the highest conversion efficiencies of all thin film solar cells, above 19%. Solar cells based on these materials are also very stable, thus allowing long operational lifetimes. The preparation of a thin film solar cell is a multistage process where every step affects the resulting cell performance and the production cost. $CuInSe_2$ and other Cu chalcopyrites can be prepared by a variety of methods, ranging from physical vapor deposition methods such as evaporation and sputtering to low-temperature liquid phase methods such as electrodeposition. The present review discusses first the concept and operation principle of thin film solar cells, as well as the most important thin film solar cell materials. Next, the properties of $CuInSe_2$ and related compounds, as well as features of solar cells made thereof are reviewed. The last part of the text deals with deposition methods used for the preparation of $CuInSe_2$ and $Cu(In,Ga)Se_2$ thin film absorbers and solar cells. Although the emphasis here is on absorber preparation methods, buffer and conducting oxide preparation are discussed as well.

Keywords photovoltaics, copper chalcopyrites, absorber layer, buffer layer, transparent conducting oxide

Table of Contents

*E-mail: marianna.kemell@helsinki.fi

LIST OF SYMBOLS AND ABBREVIATIONS

λ	Wavelength
η	Efficiency
ALD	Atomic layer deposition
CBD	Chemical bath deposition
CVD	Chemical vapor deposition
MOCVD	Metal organic chemical vapor deposition
AA-MOCVD	Aerosol-assisted metal organic chemical vapor deposition
AP-MOCVD	Atmospheric pressure metal organic chemical vapor deposition
LP-MOCVD	Low-pressure metal organic chemical vapor deposition
e	Elemental charge (1.602×10^{-19} C)
E	Standard potential
E_C	Conduction band
E_F	Fermi level
E_g	Band gap
E_V	Valence band
FF	Fill factor
$h\upsilon$	Photon energy
I	Current
I_{dark}	Dark current
I_{mp}	Photocurrent at the maximum power point
I_{ph}	Photocurrent
I_{sc}	Short circuit current
ILGAR	Ion layer gas reaction
ITO	Indium doped tin oxide, SnO_2:In
j	Current density
j_{dark}	Dark current density
j_{mp}	Photocurrent density at the maximum power point
j_{ph}	Photocurrent density
j_{sc}	Short circuit current density
K_s	Solubility product
MBE	Molecular beam epitaxy
N_A	Acceptor concentration
ODC	Ordered defect compound
OVC	Ordered vacancy compound
P_{max}	Maximum power point
PLD	Pulsed laser deposition
PVD	Physical vapor deposition
RT	Room temperature
TCO	Transparent conducting oxide
V_f	Forward bias
V_{oc}	Open circuit voltage
V_r	Reverse bias
XRD	X-ray diffraction

1. INTRODUCTION

Most of the present global energy production is accomplished by burning fossil fuels. However, the inherent problems associated with the use of fossil fuels such as their limited availability and the environmental issues force mankind to look for new, more sustainable long-term energy solutions to provide the future energy supply.

One of the most powerful alternatives for future large-scale electricity production is photovoltaics, that is, the conversion of sunlight directly into electricity. Sunlight is available in most locations, and it provides such an enormous supply of renewable energy that if the whole global electricity demand would

be covered exclusively by photovoltaics, the total land area needed for light collection would be only a few percent of the world's desert area.[1,2] Solar cells are easy to install and use, and their operational lifetimes are long, which eliminates the need for continuous maintenance. Because photovoltaic systems are modular, they are equally well suited for both centralized and non-centralized electricity production. Therefore their potential uses range from simple consumer electronics (pocket calculators, wrist watches, etc.) to large power plants.

Due to its reliability and stability, solar energy combined with short-term storage devices is a good choice in applications where power outages or shortages cannot be tolerated, for example in hospitals and certain production plants. Photovoltaic systems can be installed on rooftops and façades of buildings, and they can be combined with solar water heating systems. The power generated by rooftop solar cells can be used locally, and the surplus can be exported to the commercial grid if there is one in the region.[2,3] The possibility for local electricity production offers consumers more freedom by reducing their dependence on the availability and price of commercial electricity. This is a crucial feature, especially in remote areas that lack the infrastructure of electrification. One calculation shows that it is more cost-effective to install a photovoltaic system than to extend the grid if the power requirement lies more than about half a kilometer away from the electrical line.[4] Rooftop photovoltaic installations, both by public institutions and by individual citizens, are becoming more and more common worldwide.[3,5]

One of the main obstacles for photovoltaics to become more popular in the short term is the fact that the price of the electricity (cost per watt) produced by photovoltaics is in most cases not yet competitive with that produced by the conventional methods. Cost reduction can be achieved by either improving the efficiencies or reducing the production costs of photovoltaic modules. The production costs will obviously go down with increasing production volumes.

Among the most promising absorber materials for solar cells are $CuInSe_2$-based chalcopyrite materials (copper indium selenide, CIS). The material properties can be varied by replacing part of the indium by gallium and/or part of the selenium by sulfur to form $Cu(In,Ga)(S,Se)_2$. Conversion efficiencies higher than 19%[6] have been achieved using these materials. Moreover, CIS-based solar cells are very stable, and thus their operational lifetimes are long. The favorable optical properties of these materials (direct energy band gap and high absorption coefficient) allow the use of thin films (few micrometers) instead of thick slices of bulk silicon. This reduces the consumption of materials. CIS-based thin films can be prepared both from gas and liquid phases by a variety of methods.

A number of reviews exist that deal with different aspects of solar energy, such as solar cell materials and structures.[2,4,7–13] Properties of copper chalcopyrites have been reviewed as well.[14–19] In this review, the main focus is on thin film deposition methods used for CIS-based solar cells. Deposition methods for absorber, buffer, and conducting oxide layers are reviewed separately from each other. Prior to the deposition methods, general aspects of thin film solar cells as well as properties of $CuInSe_2$ and related compounds are briefly discussed.

2. THIN FILM SOLAR CELLS

Solar cells, or photovoltaic devices, are devices that convert sunlight directly into electricity. The power generating part of a solid-state solar cell consists of a semiconductor that forms a rectifying junction either with another semiconductor or with a metal. Thus, the structure is basically a pn-diode or a Schottky diode. In some junctions, a thin insulator film is placed between the two semiconductors or the semiconductor and the metal, thereby forming a semiconductor-insulator-semiconductor or a metal-insulator-semiconductor junction. Moreover, pn-junctions may be classified into homojunctions and heterojunctions according to whether the semiconductor material on one side of the junction is the same as or different from that on the other side. Also liquid-junction solar cells exist where the junction is formed between a semiconductor and a liquid electrolyte. Thin film solar cells are usually pn- or pin-diodes, and therefore only these types of devices are discussed here in more detail.

When the junction is illuminated, the semiconductor material absorbs the incoming photons if their energy $h\upsilon$ is larger than that of the band gap of the semiconductor. The absorbed photons are converted into electron-hole pairs. These photogenerated electron-hole pairs are separated by the internal electric field of the junction: holes drift to one electrode and electrons to the other one.[4,13] The electricity produced by a photovoltaic device is direct current and can be used as such, converted into alternating current, or stored for later use.

Figure 1 presents a schematic energy band diagram of a pn-heterojunction solar cell (a) at thermal equilibrium in dark, (b) under a forward bias, (C) under a reverse bias, and (d) under illumination, open circuit conditions. Numbers 1 and 2 in Figure 1 refer to an n-type and a p-type semiconductor, respectively, and E_{Ci} and E_{Vi} to their conduction and valence bands, respectively. E_{gi} and E_{Fi} are the band gaps and Fermi levels, respectively. In the absence of an applied potential (Figure 1a), the Fermi levels of the semiconductors coincide, and there is no current flow. A forward bias V_f (Figure 1b) shifts the Fermi level of the n-type semiconductor upward and that of the p-type semiconductor downward, thus lowering the potential energy barriers of the junction, and facilitating the current flow across it. The effect of a reverse bias V_r (Figure 1c) is opposite: it increases the potential barriers and thus impedes the current flow. Illumination of the junction (Figure 1d) creates electron-hole pairs, causing an increase in the minority carrier concentration. The Fermi levels re-adjust so that the potential energy barrier decreases, and a photovoltage V_{OC} (photovoltage under open circuit conditions, or open circuit voltage) is generated across the junction.[4,7]

Solar cells are characterized by current-voltage (I–V) measurements in the dark and under standardized illumination that simulates the sunlight.[20,21] Figure 2 shows an example of diode

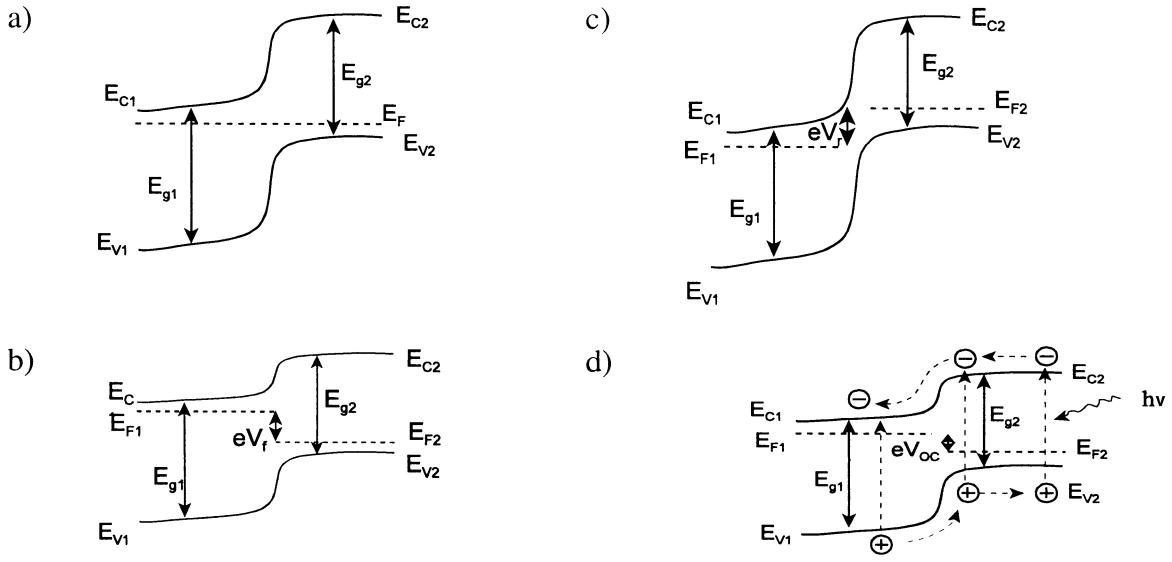

FIG. 1. A simplified energy band diagram of a pn-heterojunction solar cell (a) at thermal equilibrium in dark (b) under a forward bias (c) under a reverse bias, and (d) under illumination, open circuit conditions.

characteristics of a solar cell in the dark and under illumination. The most important parameters that describe the performance of a solar cell (open circuit voltage V_{OC}, short circuit current density j_{SC}, and fill factor FF) are derived from the I-V curve measured under illumination.

The open circuit voltage is limited by the band gap energy E_g of the absorber material, and its maximum value is calculated by dividing the band gap energy by the charge of an electron (E_g/e). Because of electron-hole pair recombination, the open circuit voltages of real solar cells are considerably below their maximum limits. The maximum value of a short circuit current density, in turn, is the photogenerated current density j_{ph}[13] that depends on the amount of absorbed light. As already noted, to be absorbed the photons must have an energy $h\upsilon = hc/\lambda$ that exceeds the band gap of the semiconductor, i.e., the wavelength of the light must be short enough ($\lambda < hc/E_g$). Fill factor, which describes the shape of the illuminated I–V curve, is expressed according to the following equation:

$$FF = \frac{V_{mp}j_{mp}}{V_{OC}j_{SC}} \quad [1]$$

where V_{mp} represents the photovoltage and j_{mp} the photocurrent at the maximum power point P_{max}. The conversion efficiency η of a solar cell is the ratio of the maximum power output that can be extracted from the device ($P_{max} = V_{mp}j_{mp}$) to the incoming power (P_{in}):

$$\eta = \frac{V_{mp}j_{mp}}{P_{in}} \quad [2]$$

Based on these considerations, the band gap value is one of the most important properties of the absorber material of a solar cell. The optimum band gap value for the absorber material of a single-junction solar cell is about 1.5 eV, which results in a theoretical maximum efficiency of 30%.[13] This is because V_{OC} and FF increase, and j_{SC} decreases with increasing band gap.[4] Even higher efficiencies can be achieved with tandem solar cell structures or by using solar irradiation concentrators, but both of those approaches are out of the focus of the present review.

Most commercial solar cells of today are made of mono- or polycrystalline silicon. Silicon is a very abundant and well-known material of which a lot of experience has been gained over the decades—the first pn-junction solar cell based on crystalline silicon was made in the 1950s.[22] Silicon photovoltaics owes a lot to the microelectronics industry that has gained the knowledge of the material properties as well as developed the manufacturing techniques. Additionally, high-quality source material has been available at a relatively low price.[12,13]

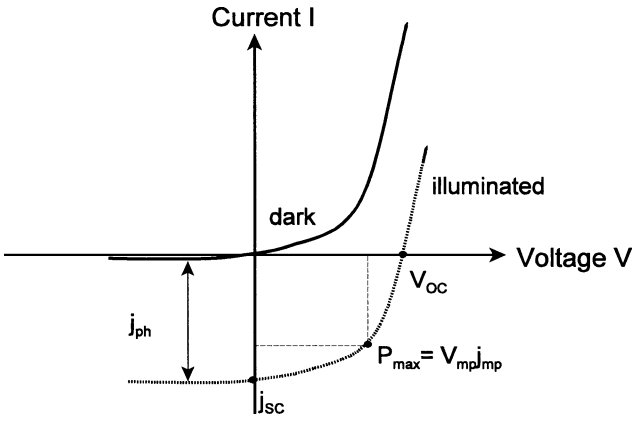

FIG. 2. Current-voltage characteristics of a solar cell in dark and under illumination.

However, owing to its indirect band gap, silicon is not an ideal absorber material for solar cells. Semiconductor materials with indirect band gaps do not absorb light as efficiently as those with direct band gaps, and therefore a thick layer of material is needed to achieve sufficient light absorption. For example, 100 μm of crystalline silicon is needed for 90% light absorption in comparison with 1 μm of GaAs that is a direct band gap semiconductor.[12] An inevitable result of such a large thickness is that the silicon used in solar cells must be of high quality in order to allow for minority carrier lifetimes and diffusion lengths long enough so that recombination of the photogenerated charge carriers is minimized, and they are able to contribute to the photocurrent. These strict material requirements increase the production costs. Moreover, due to the current production technologies, material losses during the fabrication of silicon solar cells are high.

The high production costs of crystalline silicon solar cells are compensated by their high efficiencies—the record efficiency for a small area crystalline Si solar cell is about 25%.[23] Moreover, since the 1950s, an important application of silicon solar cells has been as power sources in space vehicles where reliability and high efficiency are far more important issues than the cost. Also other, even more expensive high-efficiency materials, such as GaAs and InP are used in space applications.[2]

Due to the limitations of crystalline silicon, other absorber materials have been extensively studied. These are semiconductors with direct band gaps and high absorption coefficients, and consequently they can be used in thin film form. Thin film solar cells have several advantages over crystalline silicon cells.[12] The consumption of materials is less because the thicknesses of the active layers are only a few micrometers. Therefore, impurities and crystalline imperfections can be tolerated to a much higher extent as compared to crystalline silicon. Thin films can be deposited by a variety of vacuum and non-vacuum methods on inexpensive substrates such as glass. Also curved and/or flexible substrates such as polymer sheets can be used, leading to lighter modules. Furthermore, composition gradients can be created in a more controllable manner.

The main candidates for low-cost thin film solar cell materials are amorphous hydrogenated silicon (a-Si:H), CdTe (cadmium telluride) and $CuInSe_2$ and its alloys with Ga and/or S.[10,11] Of these, amorphous silicon solar cells currently have the largest market share.[3] The absorption coefficient of amorphous silicon is higher than that of crystalline silicon, which enables its use in thin film form, and its band gap is closer to the ideal value of about 1.5 eV. A serious disadvantage is the light-induced degradation of solar cells made of this material, which leads to a drop of conversion efficiency from the initial value.[13] This Staebler–Wronski effect results from defects (dangling bonds) created by illumination that act as recombination centers. The stabilized efficiencies of amorphous silicon solar cells are about 13%.[10]

The polycrystalline compound semiconductor materials (CdTe and $Cu(In,Ga)(S,Se)_2$) do not suffer from light-induced degradation. In fact, the performances of CIS-based solar cells have even shown some improvement after illumination under normal operating conditions.[18,24] Another advantage is that they are direct band gap materials with high absorption coefficients. The band gap of CdTe (1.4 eV) is very close to the ideal value. Despite that, the record efficiency for CdTe solar cells is only 16.5%,[23] about half of the theoretical value.

3. $CUINSE_2$ SOLAR CELLS

The Cu-chalcopyrites exhibit the highest efficiencies among thin film solar cells—the present record efficiency is 19.2% for a device with a $Cu(In,Ga)Se_2$ (CIGS) absorber.[6] An additional advantage of the Cu-based absorber materials is that they do not have the acceptability problems associated with CdTe because these materials are less toxic.[25] Nevertheless, the Cd issue is somewhat shared also by the $Cu(In,Ga)(Se,S)_2$ technology because a CdS buffer layer is commonly used. The amount of Cd is, however, much less in the $Cu(In,Ga)(Se,S)_2$ solar cells than in the CdTe solar cells because the CdS layer is very thin. Furthermore, alternative buffer layer materials are being developed, as will be reviewed in section 4.2.

Figure 3 shows a schematic representation of a CIGS substrate solar cell. Cell preparation starts by the deposition of the Mo back contact on glass, followed by the p-type CIGS absorber, CdS or other weakly n-type buffer layer, undoped ZnO, n-type transparent conductor (usually doped ZnO or In_2O_3), metal grids and antireflection coating. Finally, the device is encapsulated to protect it against its surroundings.

The structure of a CIGS solar cell is quite complex because it contains several compounds as stacked films that may react

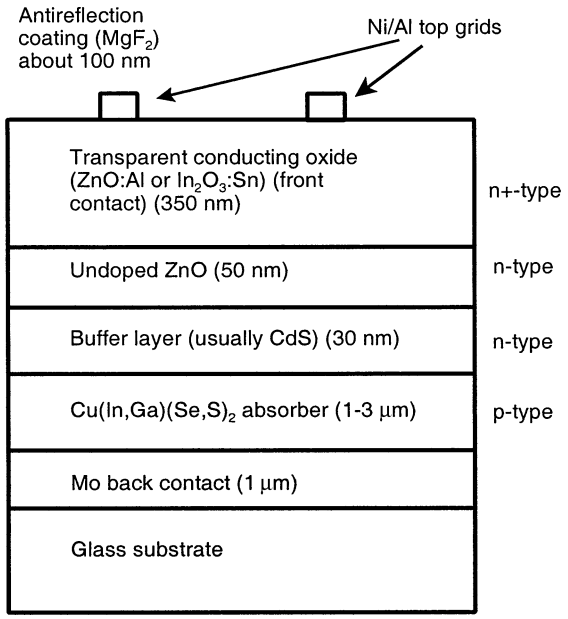

FIG. 3. A schematic view of the CIGS substrate solar cell structure.

with each other. Fortunately, all detrimental interface reactions are either thermodynamically or kinetically inhibited at ambient temperatures.[14] The formation of a thin p-type $MoSe_2$ layer between the Mo and the absorber that occurs during the absorber preparation at sufficiently high temperatures under $(In,Ga)_xSe_y$-rich growth conditions[14,26] is beneficial for the cell performance for several reasons. First, it forms a proper ohmic back contact. The Mo/CIGS contact without the $MoSe_2$ layer is not ohmic but a Schottky type contact that causes resistive losses.[26,27] The second advantageous consequence of the $MoSe_2$ interface layer is improved adhesion of the absorber to the Mo back contact. Third, because the band gap of $MoSe_2$ is wider (about 1.4 eV[26]) than that of a typical CIGS absorber, it reduces recombination at the back contact,[26,28–30] providing simultaneously a low-resistivity contact for holes.[28] Fourth, the $MoSe_2$ layer prevents further reactions between CIGS and Mo.[14]

A moderate interdiffusion of CdS and CIGS, which occurs to some extent,[31,32] is potentially beneficial to the cell performance.[14] Furthermore, the reaction of CdS with CIGS to form detrimental Cu_2S is inhibited as long as photovoltaic-quality (Cu-poor) material is used. Similar stability is not present at a CIGS/ZnO interface because Cu-poor CIGS may react with ZnO to form ZnSe and In_2O_3 or Ga_2O_3.[14] This, in addition to the sputter-induced damage during ZnO deposition (see section 4.3.2), may contribute to the lower efficiencies of buffer-free devices.[14]

Figure 4 shows the structure of an alternative, inverted configuration. The preparation of this so-called superstrate cell starts with the deposition of the transparent conductor, followed by the absorber deposition. The CdS layer is usually omitted in modern superstrate cells because the high absorber deposition temperatures would cause its intermixing with the CIGS layer.[33,34] The advantages of the inverted configuration include lower cost, easier encapsulation, and the possible integration as the top cell in future tandem cells.[34] The conversion efficiencies achieved by superstrate cells are, at least so far, between 11 and 13%, that is, several percentage units lower than those of the substrate cells.[35] This may be partly due to the fact that the substrate cells have been studied to a much greater extent than the superstrate cells.

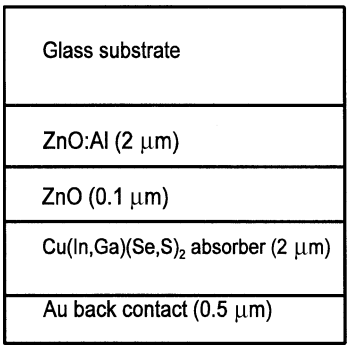

FIG. 4. A schematic view of a CIGS superstrate solar cell structure.

Because of these reasons, superstrate cells are not considered here in more detail.

3.1 Crystal Structure and Band Gap of the Absorber Material

The ternary Cu-chalcogenides crystallize most often in the tetragonal chalcopyrite structure[36] that is shown in Figure 5.[37] Sometimes, however, the cubic sphalerite phase,[38] a disordered form of the chalcopyrite, is observed. Also metastable structures with CuAu or CuPt ordering are possible, as reviewed recently by Stanbery.[17] The band gap of $CuInSe_2$ is relatively low, 1.04 eV, but it can be adjusted to better match the solar spectrum by substituting part of In by Ga or part of Se by S. The flexibility of the material system allows in principle the band gap variation from 1.04 eV of $CuInSe_2$ via 1.53 eV of $CuInS_2$ and 1.7 eV of $CuGaSe_2$ (CGS) to 2.5 eV of $CuGaS_2$.[11]

3.2 Effect of Absorber Composition on Solar Cell Performance

Although the Ga and S contents of the absorber affect the solar cell properties significantly, the most essential factor that

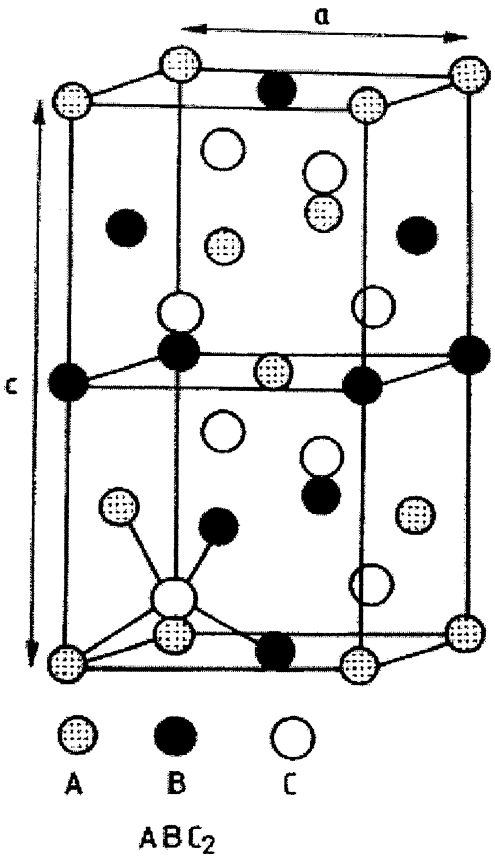

FIG. 5. Crystal structure of chalcopyrite CIGS. A = Cu, B = In, C = Se.[37] Reprinted from *J. Appl. Phys.*, 80, Merino et al., Composition effects on the crystal structure of $CuInSe_2$ layers for solar cells, 5610–5616, © 1996 American Institute of Physics, with permission from American Institute of Physics.

decides if the absorber is going to result in a high-efficiency device, is its Cu content, or the Cu/(Ga+In) ratio. Therefore, this is discussed first, followed by the effect of the Ga/(Ga+In) ratio. The effects of the sulfur content as well as different sulfurization treatments will be discussed in section 4.1.2. Finally, it must be noted that most of the considerations in this section are based on results achieved with absorbers prepared by co-evaporation and may thus not necessarily apply to other preparation methods. The high amount of literature on co-evaporated absorbers reflects the importance of this deposition method: the film composition can be adjusted quite freely, and the resulting films are usually of high quality (high crystallinity, low impurity contents, etc.)

3.2.1 Cu/(Ga+In) Ratio

For high-efficiency solar cells, the overall composition of the $Cu(In,Ga)Se_2$ absorber film should be slightly Cu-deficient, with a thin, even more Cu-deficient surface layer. The composition of this surface layer corresponds to the stable ordered vacancy or ordered defect compound (OVC/ODC) $Cu(In,Ga)_3Se_5$.[9,18,39] The formation of the OVC layer occurs automatically on the top surfaces of slightly Cu-deficient $Cu(In,Ga)Se_2$ thin films at high deposition temperatures when the In/(In+Cu) ratio in the bulk of the film is higher than 0.52.[39] Thus there is a significant difference between the bulk and surface compositions of photovoltaic-quality $Cu(In,Ga)Se_2$ films. It has been suggested[40] that the OVC layer might form only on co-evaporated absorbers. Recently, Canawa et al.[41] reported the formation of a Cu-poor surface layer after etching co-evaporated CIGS absorbers with aqueous Br_2 and KCN solutions. The composition of this surface layer was close to $Cu(In,Ga)_3Se_5$. This was the first time when the OVC layer was detected in etched material, and may thus open new possibilities for the preparation of high-efficiency absorbers.

The OVC surface layer is weakly n-type,[39] and because the bulk of the absorber is p-type, they form a buried pn-junction.[18,39,42] Thus the bulk of the CIGS absorber is p-type whereas the surface is n-type. The inverted surface minimizes the recombination at the CIGS/CdS interface.[42] The thickness of the OVC layer was found to vary from 5 to 60 nm with the Cu content of the film: the more Cu-poor the CIS film, the thicker the OVC layer.[40]

Deliberately prepared, 400 nm thick OVC layers have been reported to result in deteriorated device performances[43] which was attributed to increased series resistance because of the low conductivity of the OVC, and to light absorption in the OVC instead of the junction region. The band gap of the surface layer is direct and wider than that of the bulk; values between 1.23[44] and 1.3 eV[39] have been observed, in agreement with the value predicted from calculations, 1.21 eV.[45] The wide band gap of the surface layer increases further the barrier for recombination at the CIGS/CdS interface,[28] and is thus the key to high-efficiency solar cells.

3.2.2 Ga/(Ga+In) Ratio

One would expect that the higher band gap absorbers of the $Cu(In,Ga)(S,Se)_2$ system would result in devices with higher conversion efficiencies, but this is not the case—conversion efficiencies achieved by $CuInS_2$ ($E_g = 1.53$ eV) or $CuGaSe_2$ ($E_g = 1.7$ eV) absorbers are considerably lower than those achieved by $Cu(In,Ga)Se_2$ or even $CuInSe_2$. For comparison, the highest total area conversion efficiencies for $CuInSe_2$, $CuGaSe_2$, and $CuInS_2$ absorbers are 14.5%,[46] 9.5%,[47] and 11.1%,[48] respectively. The absorbers of high-efficiency devices are $Cu(In,Ga)Se_2$ with relatively low Ga content. For instance, the Ga/(Ga+In) ratio in the record efficiency (19.2%) absorber varies between about 15–50% as a function of depth, and the resulting band gap is 1.12 eV.[6] In other high-efficiency devices, the Ga/(Ga+In) ratio is often between 25–30%, and the band gap usually between 1.1 and 1.2 eV.[49–53]

The success of the low band gap absorbers ($CuInSe_2$ and $Cu(In,Ga)Se_2$ with a low Ga content) as compared to the wide band gap absorbers ($CuInS_2$ and $CuGaSe_2$) is partly due to historical reasons, that is, the longer research history of $CuInSe_2$ and $Cu(In,Ga)Se_2$ solar cells. There are, however, also some fundamental differences between the low and wide band gap materials.[19] These issues will be discussed shortly.

In agreement with the doping pinning rule of Zhang et al.,[54] $CuInSe_2$ and $CuInS_2$ can be either p-type or n-type, depending on the composition. $CuGaSe_2$, in contrast, is always p-type, which prevents the formation of the inverted surface.

The usefulness of $CuInS_2$, in turn, is limited by the difficulty to prepare this material with a Cu-deficient composition: attempts to prepare Cu-deficient $CuInS_2$ lead often to the formation of n-type $CuIn_5S_8$.[19] Therefore, in order to obtain high-quality $CuInS_2$, it has to be prepared under strongly Cu-rich growth conditions. The excess CuS is removed by CN^- etch after deposition before proceeding further in solar cell preparation.[48] The Cu/In ratio in the sulfide absorber is 1.0 after the CN^- etch,[48] that is, the material becomes stoichiometric. However, as explained earlier, the formation of the OVC layer requires an overall Cu-poor absorber composition. Because the OVC layer seems to be very important for high-efficiency cells,[55] absorbers prepared under Cu-rich conditions are unlikely to result in as high efficiencies as those prepared under Cu-poor conditions.

The significant impact of the Cu/In ratio is reflected in the differences between recombination mechanisms of Cu-rich and Cu-poor absorbers: according to Rau et al.,[55–57] recombination in the bulk of the absorber is the main loss mechanism in devices with Cu-poor absorbers, whereas recombination at the $Cu(In,Ga)(Se,S)_2$/CdS interface dominates in all devices where the absorber composition is Cu-rich. This behavior is independent of the size of the band gap of the absorber,[57] and can be explained in terms of the OVC that is present on the surfaces of Cu-poor absorbers, but not on the surfaces of Cu-rich absorbers.[55–57] The valence band edge of the OVC layer is lower than that of $Cu(In,Ga)(Se,S)_2$, which increases the barrier for interface recombination.[55] The activation energy for

recombination increases as a function of the band gap for Cu-poor absorbers.[55–57] For Cu-rich devices, the activation energy is smaller and almost independent of the band gap.[55–57] As a conclusion, the dominant recombination mechanism is affected by the Cu/In ratio, and not by Ga/In or Se/S ratios.[57]

Sometimes tunneling across the CIGS/CdS interface plays a role in recombination.[58,59] Tunneling may enhance both interface and bulk recombination. According to Turcu and Rau,[57] also the extent of tunneling depends on the Cu/In ratio: Cu-rich absorbers show more tunneling than Cu-poor absorbers. For Cu-poor absorbers, the extent of tunneling increases with increasing charge density, either due to doping density or defect density.[59] Increased recombination losses observed in $CuGaSe_2$ solar cells as compared to $CuInSe_2$ or $Cu(In,Ga)Se_2$ solar cells have been explained to originate from increased contribution of tunneling to the recombination in the bulk of the absorber.[58,59]

For Cu-poor material, the open circuit voltages of the cells correlate inversely with the defect densities of the absorbers, measured by admittance spectroscopy.[19,59] This is particularly manifested by the fact that the open circuit voltages of $CuInSe_2$ solar cells increase linearly with the addition of Ga to the absorber, until a Ga/(Ga+In) ratio of about 30% and a band gap of about 1.2 eV is reached. The increase of the open circuit voltage is faster than that of the band gap, and is accompanied by a decreasing defect density. Beyond the Ga/(Ga+In) ratio of about 30%, the increase of V_{OC} slows down,[59,60] accompanied by an increase of the defect density.[59,61] Thus the optimum composition of a CIS-based absorber film seems to be $Cu(In,Ga)Se_2$ with a Ga/(Ga+In) ratio of about 25–30%. The Ga content and therefore the band gap of the absorber is usually graded in such a way that the regions close to the Mo back contact contain more Ga than those closer to the film surface.[9] An example of such a graded band gap structure is shown in Figure 6. This grading enhances the separation of the photogenerated charge carriers and reduces recombination at the back contact,[62,63] which is particularly important when aiming toward reduced absorber thicknesses.[64] On the other hand, as explained in section 3.2.1., high-efficiency CIGS absorbers have a Cu-poor surface layer the band gap of which is slightly wider than that of CIGS. Therefore, the graded band gap structure of the absorber resembles the

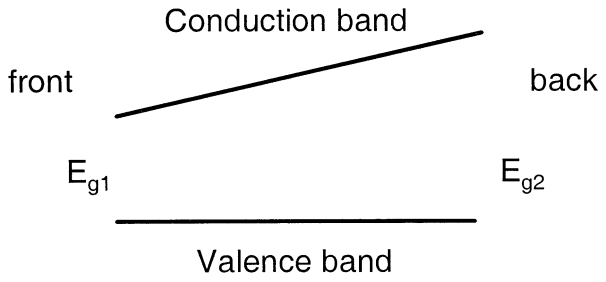

FIG. 6. A schematic representation of a graded band gap structure showing the increase of the band gap with increasing Ga/In ratio toward the back contact. Drawn after Ref. 62.

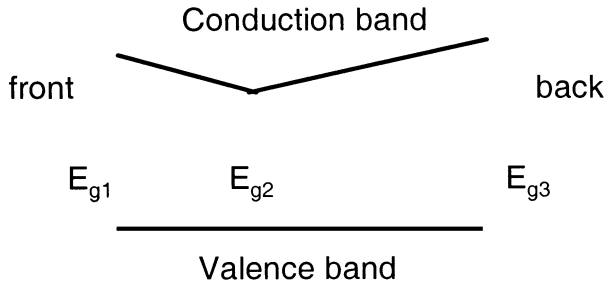

FIG. 7. A schematic representation of a double graded band gap structure showing the increase of the band gap toward both back and front contacts. Drawn after Ref. 62.

structure presented in Figure 7. In addition to the contribution of the Cu-poor surface layer, further widening of the band gap toward the front contact may be accomplished either by an increasing Ga/In ratio toward the front contact[62] and/or by surface sulfurization (see section 4.1.2.).

Moreover, as already explained, because the open circuit voltage increases and the short circuit current decreases as a function of the band gap, careful design of the grading profile allows a separate optimization of the open circuit voltage and short circuit current density: the higher band gap value of the graded material determines the open circuit voltage and the lower value the short circuit current density.[62,65]

3.3 Stability and Defect Chemistry of CIGS

In addition to the conversion efficiency, another crucial issue of a solar cell is its stability because they both affect the cost of the electricity produced, and thus the energy payback time. Despite the complexity of the CIGS solar cell structure, CIGS solar cells have shown exceptionally stable performances both under normal operating conditions[18,24] as well as under harsh conditions such as irradiation by X-rays,[66] electrons,[67–69] or protons.[68,70,71] Radiation hardness demonstrates the suitability of CIGS cells also to space applications.

3.3.1 Defect Chemistry

Besides the interfacial stability discussed earlier, the most important factors that contribute to the electrical and chemical stability of the CIS-based solar cells are the unique properties of the absorber material, especially the wide single-phase domain and the fact that the doping level remains non-degenerate (below 10^{18} cm^{-3}) over a wide composition range. Both of these effects result from the strong self-compensation of the chalcopyrite compounds: defects that are caused by deviations from the stoichiometry are compensated by new defects that neutralize them, that is, formation energies of the compensating ionic defects are low. As a result, most of the defects or defect complexes are inactive with respect to the carrier recombination.[14]

According to Zhang et al.,[45] the formation energies of defects and defect complexes in $CuInSe_2$ are low. The energetically most favored isolated point defect is the copper vacancy

V_{Cu}, a shallow acceptor that contributes to the very efficient p-type doping ability of CIS. The most favorable defect complex is $(2V_{Cu} + In_{Cu})$ that prevents degenerate doping in In-rich material. Isolated In_{Cu} would be a deep donor, but the $(2V_{Cu} + In_{Cu})$ defect complex has no deep levels and is electrically neutral. Because of the high amount of $(2V_{Cu} + In_{Cu})$ complexes, they interact with each other which further lowers the formation energies. The existence of the ordered vacancy compounds (OVC) $CuIn_3Se_5$, $CuIn_5Se_8$ and so on may be explained as periodically repeating $(2V_{Cu} + In_{Cu})$ units. Other defects may be present too but their formation energies are higher.[45]

The addition of Ga to CIS affects the defect formation energies: the $(2V_{Cu} + Ga_{Cu})$ defect complex is less stable than the corresponding complex in CIS. Thus, the formation of the OVC is more difficult in CGS than in CIS or CIGS with a low Ga content,[72] which may be one reason why CGS solar cells are not as efficient as CIS or CIGS solar cells.

3.3.2 Metastable Behavior

CIGS solar cells exhibit electric metastabilities that are manifested as the increase of the open circuit voltage and improvement of fill factor upon illumination, and as the increase of junction capacitance upon reverse biasing.[73] Illumination-induced metastabilities may occur both in the absorber and at the CIGS/CdS interface, depending on the wavelength of illumination.[14,73] Effects caused by long-wavelength (red) illumination are related to the CIGS absorber because the low energy red light is mostly absorbed in CIGS. Red illumination causes a metastable increase of net carrier concentration, which decreases the width of the space charge layer in the absorber. The open circuit voltage increases due to the reduced recombination in the narrower space charge layer.[73] Thus the increase of the open circuit voltage upon illumination is related to the CIGS absorber.[14,73]

Short-wavelength illumination (blue light), in turn, affects mostly the regions at or close to the CdS/CIGS interface. Blue light is to a great extent absorbed into the buffer layer, and the photogenerated holes are injected into the near-surface region of the CIGS absorber.[73] Illumination by blue light has been reported to improve the fill factor, which probably results from the ionization of deep donors in CdS. The positively charged fixed donors cause downward band bending in the CdS and reduce the barrier height to electrons.[14,74] The photogenerated holes have also been suggested to neutralize the negative defect states that are present on the CIGS surface.[73] The improvement of the FF upon illumination is therefore related to the CIGS/CdS interface.

Reverse bias has the opposite effect, and because it can be counterbalanced by blue illumination, it is reasonable to attribute also the effect of reverse bias to the interface region. Reverse bias generates negative charge states to the buffer layer and to the surface layer of CIGS. These negative charges may be neutralized by blue illumination.[73]

Thus the illumination-induced defect reactions are beneficial to the device performance. Moreover, the effects disappear when the device is kept in the dark overnight.[14,73] This occurs already at ambient temperatures which is beneficial because it prevents accumulative long-term damage.[14]

3.3.3 Radiation Hardness

Radiation hardness has also been suggested to be due to the self-repair of the radiation-induced damages rather than due to the resistance of the material to damage. The self-healing mechanism is a result of the mobility of Cu and reactions involving Cu-related defects and defect complexes.[75] Thus the electrical stability of the CIGS and related materials seems to be of dynamic nature rather than static. The material is not resistant to changes but it is flexible because of inherent self-healing mechanisms. Particularly, the mobility of Cu, as well as the high defect density of CIGS, are actually advantages because they help in repairing damages, thus contributing to the unusual impurity tolerance and radiation hardness. Also the Cu-poor surface composition of photovoltaic-quality CIGS films has been proposed to result from the migration of Cu in the electric field of the space charge region.[14]

3.4 Sodium and Oxygen in CIS-Based Solar Cells

Yet another interesting feature is the beneficial effect of sodium on the structural and electrical properties of Cu-chalcopyrite thin films. The phenomenon was discovered in 1993[76,77] when solar cells prepared on soda lime glass substrates showed considerably higher efficiencies than those prepared on borosilicate glass. X-ray photoelectron spectroscopy and secondary ion mass spectrometry studies revealed the presence of Na at relatively high concentrations both on the surface and in the bulk of the CIGS films deposited on Mo/soda lime glass.[76] Sodium is normally detrimental to semiconductors but its presence during the growth of CIS-based films has been reported to smoothen the surface morphology[78,79] and increase the grain size.[76–79] The latter result is somewhat questionable, however, because, according to a recent study[80] the grain size decreases in the presence of Na. Increase in carrier concentration, leading to a higher p-type conductivity,[81–85] as well as enhanced crystallinity and (112) orientation[76–79,81,82] have also been reported in CIS thin films prepared in the presence of Na. On the other hand, Rudmann et al.[80] did not find significant change of orientation upon addition of Na in most cases. Hanna et al.,[86] in turn, reported enhanced (112) orientation only with high Na doses or in the absence of Na. Further, sodium has been observed to suppress the diffusion of Ga and In,[80,87] which helps to achieve a graded Ga content. Sodium has also been suggested to aid the formation of the beneficial $MoSe_2$ layer between Mo and CIGS.[26] Although the details of the effect of Na still remain controversial, improved solar cell efficiencies have been obtained in its presence.[78,79,81,84]

Sodium thus affects both the growth and the electric properties of Cu-chalcopyrite films. Na^+ ions migrate from the substrate to the CIGS film along grain boundaries,[88] and their

incorporation into a CIGS film occurs via interaction with Se.[88,89] The Na contents in the CIGS films are quite high, typically about 0.1 at.% or higher.[15,81,85,88,90] According to Granata et al.,[85] the ideal Na content in CIS and CIGS films is between 0.05 and 0.5 at.% Most of the sodium is located at the film surface, near the Mo back contact, or at the grain boundaries.[79,82,84,85,88,89,91]

In an attempt to explain the influence of Na on the structural properties of CIGS films prepared by co-evaporation, Braunger et al.[88] proposed a model according to which Na^+ ions diffuse to the CIGS surface along grain boundaries and react subsequently with the elemental selenium to form sodium polyselenides (Na_2Se_x, x = 1-6, $\neq$5). When the Se partial pressure is low, mainly Na_2Se is formed. Na_2Se is a very stable compound, and therefore the release of Se from it is highly unlikely. Thus, part of Se is consumed to Na_2Se formation rather than the growth of the CIGS film. At higher Se pressures, the formation of polyselenides dominates. Because of the easier release of Se from them, polyselenides act as a Se source during the growth.

The increased p-type conductivity of Na-containing Cu-chalcopyrite films is generally attributed to the suppression of donor-type defects such as In_{Cu} [82,83,92,93] that act as majority carrier traps. On the other hand, the removal of a minority carrier trap has also been reported.[83]

As explained in section 3.3.1., the concentration of In_{Cu} in photovoltaic-quality films is high. Sodium eliminates the In_{Cu}-related donor states or inhibits their formation by occupying Cu sites, which results in an increased hole concentration.[82,90] The calculations of Wei et al.[93] support the conclusion that the main effect of sodium on the electronic properties of CIS is to reduce the amount of intrinsic donor defects. When present at low concentrations, Na eliminates first the In_{Cu} defects, which results in a higher p-type conductivity.[93] This removal of In_{Cu} antisites may lead to a more ordered structure that may explain also the enhanced (112) orientation.[82] Wei et al.[93] even propose the formation of layered $NaInSe_2$ that directs the CIS film to the (112) orientation.

Overly high Na doses are detrimental to the electronic properties because they result in the elimination of V_{Cu} acceptor states and thereby reduce the carrier concentration.[93] On the other hand, Na contents higher than 1 at.% were reported to increase the carrier densities to excessively high values (above 10^{18} cm^{-3}), which reduced the cell performances. This may be due to the formation of Na-containing compounds.[85] The formation of additional phases at too high Na concentrations has in fact been observed,[82] and it may result from the limited mutual solubility of $NaInSe_2$ and $CuInSe_2$.[93]

In most cases, the diffusion of Na into the absorber film from the soda lime glass through the Mo back contact at high deposition temperatures is considered to provide a sufficiently high Na concentration, but incorporation of Na by introducing Na-containing precursors such as NaF,[78,79,83] Na_2S,[91,92] Na_2Se,[84,94] Na_xO,[95] $NaHCO_3$[94] or elemental Na,[81] has also been studied. The advantage of this approach is the possibility of a better control over the sodium content and thus a better reproducibility because the Na supply from the glass depends on the absorber deposition process as well as on the properties of the Mo back contact[78,94] and the glass itself.[78] Thus, the amount of Na diffusing from the substrate is difficult to estimate accurately. Moreover, because the diffusion of Na from the substrate is slow at low temperatures, the deliberate addition of Na allows one to use lower deposition temperatures without degrading the cell efficiency.[79,81] For instance, the addition of NaF allowed Bodegård et al.[79] to decrease the CIGS deposition temperature from 510 to 425°C with essentially no degradation of the conversion efficiency. In another study,[81] the conversion efficiency decreased only 1.3 percentage units upon decreasing the deposition temperature from 550 to 400°C in the presence of additional sodium. In both cases, the efficiencies achieved under insufficient supply of sodium were several percentage units lower.[79,81] Furthermore, preparation of efficient superstrate cells may require the deliberate addition of Na because its diffusion from the glass is blocked by the transparent conductor[34] or the thin SiO_2 layer that is often present between the glass and the commercial conducting oxide thin films.[96,97]

Effects of other alkali metal fluorides (LiF,[79] KF,[82] and CsF[82]) have also been studied. The addition of LiF was reported to cause an increased grain size and enhanced (112) orientation but to a smaller extent than NaF. The grain sizes were comparable to those of the Na-containing films but the film surfaces were rougher.[79] The addition of KF increased the conductivity somewhat, but CsF had in some cases the opposite effect because it decreased the photoconductivity.[82] The smaller effect of LiF may result from its higher chemical stability and thereby different decomposition behavior as compared to NaF.[79] The smaller influence of KF and CsF was explained by the differences in the ionic radii: the smaller ionic radius of Na helps its substitutional incorporation into the chalcopyrite lattice.[82] Thus, NaF had the highest influence on the film properties.[79,82]

In addition to the effects discussed earlier, Na also enhances the influence of oxygen in the CIS-based films.[95,98–100] The main role of oxygen is the passivation of positively charged Se vacancies (V_{Se}) that are present at the surfaces and grain boundaries of the Cu-chalcopyrite thin films.[93,99,100] The presence of Se vacancies at grain boundaries is especially detrimental because they decrease the effective p-type doping of the film. Additionally, they act as recombination centers for the photogenerated electrons.[98–101] The passivation of Se vacancies is therefore of significance to the performance of the solar cell.[98–100] Air-annealing has been used routinely to improve the photovoltaic properties of the CIGS solar cells.[15] Physisorbed oxygen that is present at the surfaces and grain boundaries of oxygen-exposed CIGS films, chemisorbs as O^{2-}, which occupies the positively charged vacant Se sites, and thus obviates their disadvantageous effects. Sodium has been suggested to promote the formation of chemisorbed O^{2-} ions by weakening the O—O bond.[93,95,98] The correlated concentration distributions of these two elements in air-exposed CIGS films[82,84,88,91,95] support this idea. On the

other hand, a recent study[102] indicates that oxygen is needed for the diffusion of sodium from soda lime glass: suppression of Na diffusion was observed in 1×10^{-8} Torr vacuum, whereas diffusion occurred in 1×10^{-5} Torr of either air, oxygen, or water vapor.

4. THIN FILM DEPOSITION METHODS FOR $CUINSE_2$-BASED SOLAR CELLS

A wide range of preparation methods exist for the thin film materials used in the CIS-based solar cells. The deposition method has generally a large impact on the resulting film properties as well as on the production costs. In this section, the most important deposition methods are reviewed, with the main emphasis on those used for the absorber deposition. Moreover, because $CuInSe_2$ and $Cu(In,Ga)Se_2$ are the most important Cu-chalcopyrite absorber materials, they are emphasized in this presentation. To some extent the deposition methods apply to $CuGaSe_2$ and $CuInS_2$ films as well.

The preparation of a standard CIS-based solar cell involves several steps that all are important. The preparation of a normal substrate configuration Cu-chalcopyrite solar cell starts from the deposition of the 1–2 μm thick Mo back contact that is most often sputtered. The quality of the back contact and its adhesion to the underlying glass substrate are very important matters. After the deposition of absorber, buffer, and transparent conductor, metal grids (most often Al or Ni/Al) are deposited on the transparent conductor in order to enhance its conductivity. Finally, an antireflection coating (MgF_2) is added in order to minimize reflection losses and thus increase the efficiency.

4.1 Absorber Layer

Although various techniques can be used to obtain stoichiometric CIS and CIGS films, only a few of them have resulted in high efficiency (over 15%) solar cells so far. The high-efficiency absorber films are usually prepared either by co-evaporation from elemental sources or by reactive annealing of precursor films (elemental or compound layers) under selenium-containing (H_2Se or elemental Se vapor) atmospheres.[9]

In this chapter, the most important deposition methods, that is, co-evaporation and chalcogenization of metallic layers, will be reviewed first. After that, evaporation from compound sources, chemical vapor deposition, and related methods will be discussed. Finally, electrodeposition and other liquid-phase methods, as well as selenization of particulate precursor layers will be discussed.

Regardless of the deposition method, the absorber films of CIS-based high-efficiency devices have smooth surface morphologies and consist of large, densely packed grains. The films are crystalline with the chalcopyrite structure,[36] and their overall compositions are made slightly Cu-deficient, in order to enable the formation of the Cu-poor ordered vacancy compound (OVC) on the surface.[28,39] No additional phases are allowed in the films, copper selenide phases especially are detrimental to the solar cell performance because, being a degenerate semiconductor, $Cu_{2-x}Se$ is very conductive and causes high dark currents.

The formation of a photovoltaic-quality film requires generally a high temperature (400°C or above) during either the film growth or post-deposition annealing. The formation of Ga-containing phases (CGS and CIGS) requires generally higher temperatures or longer reaction times than CIS.[9,103–106] Higher temperatures also facilitate the formation of the $MoSe_2$ interlayer.[26] The formation of a Cu-rich phase during the early stages of the growth enhances the formation of smooth, dense, and large-grained films. The presence of Na during the growth has beneficial consequences, as reviewed in section 3.4. As the high process temperatures may cause a loss of Se, that must be compensated for, for instance by maintaining a Se-containing atmosphere.

4.1.1 Co-Evaporation from Elemental Sources

The most successful absorber deposition method for high-efficiency small-area devices seems to be the three-stage co-evaporation of CIGS from elemental sources in the presence of excess Se vapor.[62,107] The Se/metal flux ratio is a very important parameter that affects orientation, morphology, and grain size.[52] Deposition is often performed under ultra high vacuum conditions using a molecular beam epitaxy (MBE) system. The three-stage process, developed at the US National Renewable Energy Laboratory (NREL), is based on the bilayer process of Boeing[106] that involves the co-evaporation of a Cu-rich CIGS layer at a lower substrate temperature (450°C), followed by an In-rich layer at a higher temperature (550°C). The layers intermix, forming a homogeneous film with a slightly Cu-deficient overall composition. The flux and temperature profiles of the NREL three-stage process are shown in Figure 8. The process involves first the deposition of $(In,Ga)_2Se_3$ at a lower substrate temperature (about 300–350°C) and then the evaporation of Cu and Se at a higher temperature (500–560°C) to yield Cu-rich CIGS. After adding some more $(In,Ga)_2Se_3$, a slightly Cu-deficient final

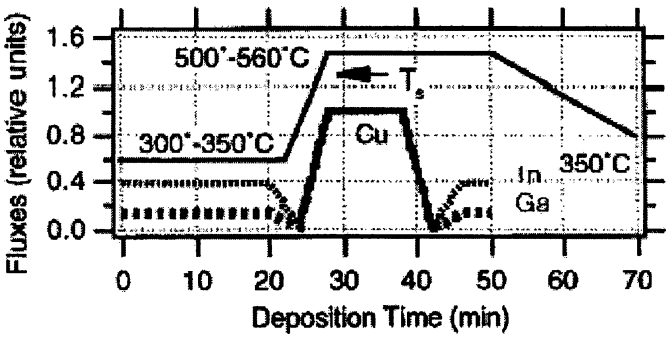

FIG. 8. Flux and temperature profiles for a three-stage co-evaporation process. Reprinted from Proc. 1st World Conf. Photovolt. Energy Conv., Contreras et al., High efficiency $Cu(In,Ga)Se_2$-based solar cells: processing of novel absorber structures, 68–75, © 1994 IEEE, with permission from IEEE.

film composition is achieved. A Se vapor treatment is carried out during the cooling step.[62] The Ga/(Ga+In) ratio is usually varied as a function of depth in order to achieve a graded band gap that improves the separation of the photogenerated charge carries and reduces recombination at the back contact as was explained in section 3.2.2. For example, in the world record cell the Ga/(Ga+In) ratio is about 50% close to the Mo back contact and about 15–20% close to the top surface.[6]

CIGS films prepared by the three-stage co-evaporation process have resulted in solar cell efficiencies close to 20% by many groups: the current[6] and previous[49] world records of 19.2%[6] and 18.8%,[49] of NREL, respectively, 18.5% of Matsushita,[50] 18.0% of Aoyama Gakuin University of Tokyo,[51] 17.6% of Tokyo Institute of Technology,[52] as well as the best Cd-free device with a CBD-ZnS buffer of 18.1%.[53]

Several variations of the three-stage process exist. Stolt et al.,[108] for example, kept the substrate temperature constant, at 500°C, during the three growth stages. Because the Se, In, and Ga fluxes were also held constant, the Cu flux was the only parameter that changed during the process. This approach led to solar cell efficiencies of about 15%. An additional advantage of this process was the high growth rate: the deposition time of 2 μm CIGS films was 20 min.[108] In another study,[109] the deposition time could be reduced even below 4 min, whereas the resulting solar cell efficiency still remained at 12.3%. The decreased efficiency was attributed to increased recombination due to the smaller grain size of the fast grown absorbers, as compared to those deposited using slower rates. For comparison, Figure 9 shows the relative evaporation rates for the various evaporation times.[109] Graded Ga content on one hand, and reduced absorber thickness of about 1 μm on the other hand, were found to improve the solar cell performances of the fast grown absorbers.[109] When the absorber deposition was started with a thin $CuGaSe_2$ layer, relatively high efficiencies were achieved with thinner absorbers as well: cells with 1 μm and 0.6 μm absorbers led to efficiencies of 15.0% and 12.1%, respectively.[64] In Ref. 109, a two-stage process was used, where the first stage was performed under Cu-rich conditions, and the second one under Cu-poor conditions. The flux ratio profile of this two-stage process is shown in Figure 10.[109] In Ref. 64, the evaporation was performed using a constant Cu/(In+Ga) flux ratio of about 0.9 throughout the entire process. The latter approach, that is, single-stage co-evaporation, is widely used, and results generally in solar cell efficiencies of about 14–16%.[40,56,64,86]

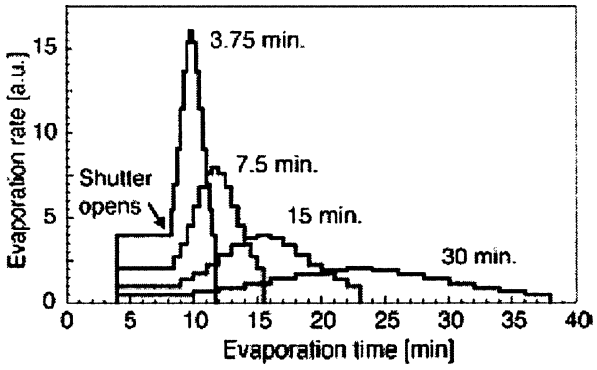

FIG. 9. Relative evaporation rates for the various evaporation times used in Ref. 109. Reprinted from *Thin Solid Films*, 431–432, Lundberg et al., Rapid growth of thin $Cu(In,Ga)Se_2$ layers for solar cells, 26–30, © 2003 Elsevier, with permission from Elsevier.

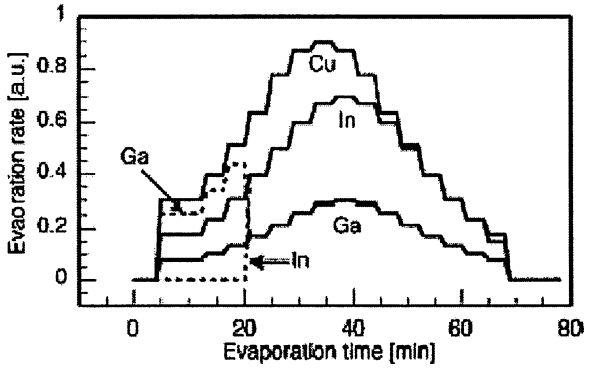

FIG. 10. Relative evaporation rates of Cu, In, and Ga in a two-stage co-evaporation process where the first stage was performed under Cu-rich conditions and the second stage under Cu-poor conditions. Dotted line shows the evaporation rates for a CIGS absorber with a graded Ga content.[109] Reprinted from *Thin Solid Films*, 431–432, Lundberg et al., Rapid growth of thin $Cu(In,Ga)Se_2$ layers for solar cells, 26–30, © 2003 Elsevier, with permission from Elsevier.

Shafarman and Zhu[110] showed that the flux ratio variation did not have a large impact on the device efficiency (best 16.4%) when the co-evaporation was done at 550°C. At 400°C, in contrast, the presence of a Cu-rich growth stage improved the device efficiencies (best 14.1%), whether in the beginning or in the middle of the deposition.

A remarkable feature in the 18.8% efficient cell of NREL in 1999[49] was that the CIGS films were (220/204) oriented—the typical orientation of chalcopyrite CIGS films is either random or (112). Nowadays, (220/204) oriented absorbers are quite common in high-efficiency devices.

In three-stage co-evaporation, the orientations of $CuInSe_2$ and CIGS thin films depend strongly on the orientation of the underlying $(In,Ga)_2Se_3$ precursor layer.[52,111] According to Chaisitsak et al.,[52] the Se/(In+Ga) flux ratio during the first stage of evaporation is the most important parameter that determines the orientation. High flux ratios increased the (220/204) orientation of CIGS by increasing the (300) orientation of the $(In,Ga)_2Se_3$ precursor. Increasing substrate temperature during the first stage was reported to have the opposite effect.[52] Properties of the Mo layer such as morphology, grain size, and stress also have an effect: (220/204) oriented $CuInSe_2$ thin films were achieved only on dense, almost pinhole-free, large-grained

Mo films with low tensile stress and a low Na content at the surface.[111] On the other hand, Rudmann et al.[80] studied the effect of Na supply, and found the orientation to remain (220/204) unless a very high Na supply was used. Under Na-free conditions[112] the film orientation was found to depend on the substrate orientation, that is, (100) oriented Mo resulted in (112) oriented CIGS and (110) oriented Mo in (220/204) oriented CIGS.

Increase of the Se/metal flux ratio has been observed to enhance the (220/204) orientation also in the single-stage co-evaporation.[86] In the same publication, the effect of Na supply during the growth was studied as well. In agreement with Rudmann et al.,[80] an increasing (112) orientation was observed with high Na doses.[86] Also the absence of Na caused the (112) orientation, whereas intermediate Na doses led to the (220/204) orientation.[86]

The (220/204) oriented films were found to be more resistive than the (112) oriented films, and their apparent band gaps were lower than those of the (112) oriented films.[112] The higher conversion efficiencies achieved with the (220/204) oriented absorbers were mainly due to increased fill factors and lower sheet resistances, whereas the j_{SC} and V_{OC} were in most cases only moderately higher.[112] According to Chaisitsak et al.[52] the increase of the efficiency from 15.5% with the (112) oriented absorber to 17.6% with the (220/204) oriented one may be explained by an easier diffusion of Cd^{2+} ions into the (220/204) oriented films during the deposition of CdS. The differences of the diffusion behavior of Cd may explain the lower series resistances that Contreras et al.[112] observed for solar cells prepared using (220/204) oriented absorbers, as compared to (112) oriented. Possible reasons for the dependence of Cd diffusion on the orientation of the CIGS film are a higher dissolution rate of Cu into the NH_3-containing CdS deposition bath from the (220) surfaces and/or the fact that there are less atoms on the (220) surface as compared to the (112) surface.[52]

Despite its unquestionable power in preparing high-quality material on small areas, co-evaporation exhibits some problems related to upscaling. This is due to the fact that co-evaporation requires a strict control of the evaporation fluxes to achieve the desired film properties such as composition, texture, and electrical properties. This is particularly difficult with large substrate areas. As an inevitable consequence, the conversion efficiencies of large area cells and modules are considerably lower than those of the smaller-area devices,[113] for example the efficiency reported by Matsushita laboratories was 12.6% for a 81.54 cm^2 submodule[114] as compared to 18% for their small-area cell.[50] Moreover, in addition to the sophisticated and expensive equipment, the high deposition temperatures and incomplete utilization of source materials add to the complexity and cost of the co-evaporation method.[113]

According to ZSW/Würth Solar,[115] the production of CIGS modules by co-evaporation should, however, be possible well below the common market price of the crystalline Si solar cell technology. Their in-line co-evaporation process[115,116] is based on one-step co-evaporation of Cu, In, Ga, and Se from elemental sources onto moving substrates at high temperatures. Efficiencies of 30 cm × 30 cm CIGS modules average 11.3%, with a maximum value of 12.7%. The maximum efficiency for a Cd-free module of the same size was 9.7%.[115]

4.1.2 Selenization of Metallic Precursor Layers

Although the difficulties in upscaling are somewhat shared by all the deposition methods, the alternative multistep approach where the absorber is prepared by combination of simple, well-established deposition techniques from the more simple precursor layers offers certain advantages: compositional uniformity over large areas may be easier to achieve, and in many cases the throughput is increased as compared to the co-evaporation. Moreover, the processes are often cost-effective because of the low deposition temperatures. This is important because apart from its efficiency and implementation, the energy payback time of a photovoltaic module depends on its production cost. For example, the energy payback time for CIS modules of Siemens Solar Industries (SSI), manufactured by selenization of metals, has been calculated to be 9 to 12 years for modules made in pilot production and about 2 years for modules made in full production. Empirical calculations show that during its lifetime (estimated to be 30 years), a CIS panel generates up to 14 times the energy required to produce it.[117]

The most common multistep method is the selenization of stacked metal or alloy layers. The metals and alloys can be deposited by a variety of methods, the most common of which are sputtering,[104,113,118–122] evaporation,[103,121,123–134] and electrodeposition.[118,122,128,133,135–142] Recently, a new approach was introduced that involves reactive sputtering of Cu-In alloy in the presence of trimethyl gallium vapor.[143] In that study, the incorporation of chalcogen into the films was done either during or after the metal precursor deposition.[143]

The metal precursors are most often deposited at or near room temperature, but higher temperatures have been used as well. In order to facilitate the interdiffusion of the metal precursors and alloy formation, the metal precursors can be pre-annealed at a lower temperature[103,121,123,127,132,138,144] prior to selenization. The reaction between sequentially evaporated Cu/Ga layers has been observed to be slower than that of similar Cu/In layers.[145] Another approach is the deposition of Cu/In/Cu/In/Cu/In . . . multilayers instead of a bilayer.[119,125,126,144] The multilayer approach has been reported to result in smoother surfaces and better crystallinity.[126] Selenization is most often carried out under a selenium-containing atmosphere at high temperatures, typically above 400°C. Selenium may be present either as H_2Se,[104,121,123,128,129,134,136,139,142–144] most often diluted by Ar, or elemental Se.[103,118–120,122,125–127,129,133,135,140] Selenization time depends on thickness, structure, and composition of the film, as well as on the reaction temperature and selenium source. Generally, the formation of CIS by selenization is faster and

occurs at lower temperatures than the formation of CGS.[103,105] As a result, CIGS films may contain CIS and CGS as separate phases if the reaction temperature is too low or the time is too short.[104] High reaction temperatures also facilitate the formation of $MoSe_2$.[26,119,129] The chalcogenization method offers also a possibility of forming $CuIn(S,Se)_2$ thin films by introducing both Se and S precursors into the annealing atmosphere.[125,144]

The influence of the chalcogenide source in selenization of evaporated Cu-In alloys at different temperatures (between 250 and 600°C) has been studied in detail by Bekker et al.[129] Three selenization methods were compared: (1) H_2Se/Ar at atmospheric pressure, (2) solid Se source under Ar flow at atmospheric pressure, (3) elemental Se vapor in vacuum. In all cases the samples were heated for 10 min to the reaction temperature, and the reaction time was 40 min. At temperatures below 500°C, the H_2Se method was found the most efficient, resulting in films with about 50 at.% Se already at 400°C. The Se vapor approach was the most inefficient. Above 500°C, a Se content of about 46–52% was achieved by all methods. Single-phase $CuInSe_2$ films were obtained only by the H_2Se method at 400°C. Additional phases, Cu and In selenides and/or Cu-In alloys, were detected in all other samples. The H_2Se method also resulted in the best compositional uniformity and the largest grain sizes. The formation of $MoSe_2$ was detected only after selenization by H_2Se at 600°C.[129] Thus, H_2Se is the most efficient selenization source but its toxicity is a serious drawback. Recently, diethylselenide was introduced as an alternative, less toxic selenium source. Promising results were obtained from the selenization experiments with Cu-In and Cu-In-O precursors.[130]

Chalcogenization can also be done by depositing the chalcogen film on or between the metallic layers, again either by evaporation[113,124,125,134,137,146] or electrodeposition[131,132,138,141] and annealing the stack under an inert atmosphere,[124,132,134,137,138] thus forming the desired compound and avoiding the use of toxic vapors such as Se and especially H_2Se. Sometimes, however, a chalcogen-containing annealing atmosphere[125,134,141,146] is required in order to compensate for the chalcogen loss at high temperatures. Alberts et al.[134] observed significant Se losses upon annealing of stacked In/Se/Cu/In/Se layers above 200°C, irrespective of whether the annealing was performed in vacuum with elemental Se vapor or under an Ar flow at atmospheric pressure in the absence of Se. No In loss was detected until above 650°C.[134]

Alberts et al.[144] studied also the two-step chalcogenization of Cu-In alloys. When the first chalcogenization was performed under a H_2Se/Ar atmosphere, and the second one under a H_2S/Ar atmosphere, a complete conversion of $CuInSe_2$ to $CuInS_2$ was observed. When the second chalcogenization was done under a H_2S/H_2Se/Ar mixture, sulfur was found mostly close to the Mo back contact and at the CIS surface. The surface concentration of sulfur was dependent on the bulk Se concentration of the films after the first chalcogenization. The films that had sulfur on the surface showed a slightly increased band gap as compared to the pure $CuInSe_2$ films.[144]

The sulfur distribution in chalcopyrite films has been found to depend strongly on the composition and microstructure of the original CIS or CIGS film.[147] The distribution was nearly uniform in copper-rich films, whereas in near-stoichiometric and indium-rich films most of the sulfur was close to the surface. In indium-rich films, sulfur was found also close to the Mo/absorber interface. The Ga content of the film affected the distribution as well: more S was found close to the Mo/absorber interface when the Ga/(Ga+In) ratio in the near-stoichiometric film was increased. In that study, the H_2S annealing time was long, 20 min, and the temperature was 575°C.[147] Surface sulfurization (10–50 min by H_2S at 350–550°C) of co-evaporated CIS and CIGS films was reported to result in surface roughening, that is, nonuniform and porous surface layers. The sulfurization of CIS films resulted in the formation of sulfoselenides below the $CuInS_2$ surface layer, and improved the cell performance. In CIGS films, a phase separation to $Cu(In,Ga)Se_2$ and $Cu(In,Ga)S_2$ occurred, and the resulting cell performance was poor.[148]

The absorber surface can be sulfurized also by liquid-phase methods. Negami et al.,[50] for example, soaked their co-evaporated CIGS absorbers in a solution containing $InCl_3$ and thioacetamide (CH_3CSNH_2) to sulfurize the surface. The thin $CuInS_2$ layer on the absorber surface increased the stability and conversion efficiency of the cell because it improved the quality of the pn-junction by passivating the surface.[149]

The process of Showa Shell[150,151] involves sputtering of stacked precursor layers (Cu-Ga alloy and In) followed by selenization with dilute H_2Se and surface sulfurization with dilute H_2S at high temperatures. The thin (about 50 nm) $Cu(In,Ga)(S,Se)_2$ surface layer is thought to improve the surface quality and thus the fill factor via the passivation of shallow defects such as selenium vacancies and Se_{Cu} antisites.[150] Module efficiency of 12.5% was achieved for an area of 859.5 cm^2.[151] A remarkable feature is that the device was Cd-free, with Zn(O,S,OH) as the buffer layer.[150,151]

The process of Siemens AG,[152] in turn, eliminates the use of toxic H_2Se gas because the absorber is prepared by depositing the constituent elements at room temperature, followed by rapid annealing under a sulfur-containing atmosphere at 550°C or lower temperatures to yield $Cu(In,Ga)(S,Se)_2$. The CIGS module preparation process is shown in Figure 11.[146] Cu-Ga and In layers were sputtered, and Se was evaporated thermally. The amount of Se exceeded the stoichiometric one by about 40% in order to compensate for the Se loss that occurs during annealing.[146,152] Moreover, the process involved a controlled Na incorporation by depositing a Na compound on Mo before the absorber deposition.[146] Module efficiency of 14.7% (average 13.2%) for 18.9 cm^2 aperture area was achieved by this process, as compared to 11.8% (average 11%) when the annealing was performed without sulfur.[152] This increase in efficiency was due to an increase of band gap and open circuit voltage of the absorber material.[152] The depth distributions of sulfur and gallium were nonuniform—their contents were the highest close

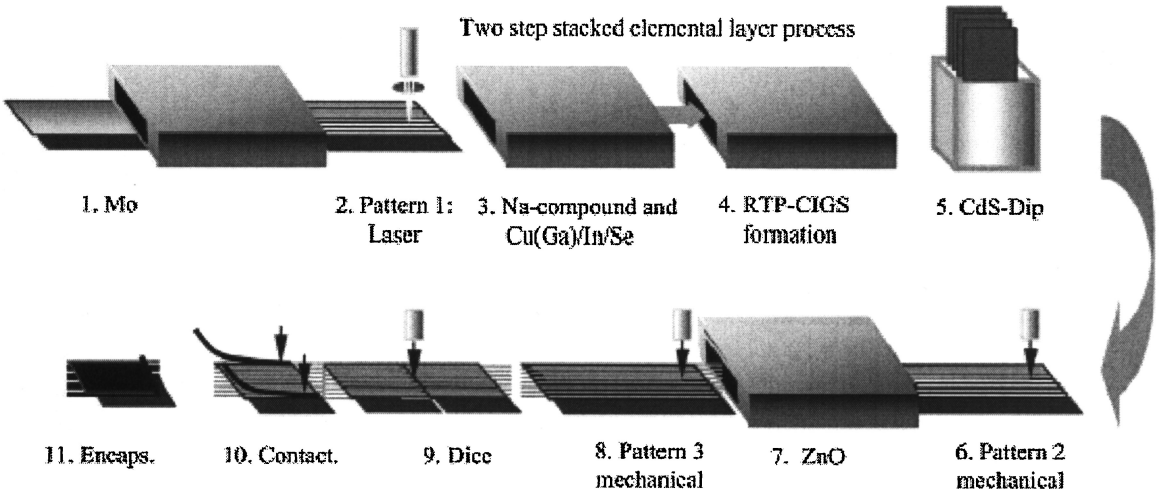

FIG. 11. Schematic representation of the Siemens CIGS module preparation process. Reprinted from *Thin Solid Films*, 387, Probst et al., Rapid CIS-processes for high-efficiency PV-modules: development towards large area processing, 262–267, © 2001 Elsevier, with permission from Elsevier.

to the Mo back contact where the absorber consisted of smaller grains than closer to the top surface. Sulfur was thus thought to incorporate preferentially at grain boundaries.[146]

The in-line process of Lockheed Martin Astronautics involves sequential sputtering of Cu, Ga, and In from elemental targets at room temperature, followed by selenization in a Se vapor at higher temperatures.[153,154] Compound formation occurs via reactions of binary selenides.[153,154] Homogeneous CIS[153] and CIGS[154] films with uniform compositions are formed over 900 cm^2 substrates. Small-area efficiencies of over 10% have been achieved on soda lime glass after post-deposition annealing of the absorbers at 560°C 1 h.[155]

4.1.3 Evaporation from Compound Sources

Binary,[156–158] ternary,[105,127,159–164] and even quaternary[161] compounds can be used as evaporation sources too. This approach is potentially simpler and easier to control than the co-evaporation from elemental sources, provided that the compounds do not decompose during heating. Very often at least Se is lost, in which case a Se atmosphere is required during deposition and/or post-deposition annealing. Decomposition may be avoided by a very fast heating to sufficiently high temperatures so that the material evaporates before it decomposes.[164] This approach is utilized for example in flash evaporation[160–164] and related methods[158] as well as in pulsed laser deposition.[165,166]

Figure 12 shows a schematic representation of a flash evaporation equipment. The powdered source material is transported to a heated evaporation boat by a feeder system that consists of a tube via which the source material is transported and a motor (often an electromagnet) that vibrates the tube mechanically.[160,162–164] Because only a small amount of the source powder reaches the boat at a time, the high boat temperature causes an instantaneous and complete evaporation of the source material.

In pulsed laser deposition (PLD), the source material is in a form of a rotating target. The target is heated by a pulsed laser beam that is focused on the target by a lens. The energy fluence of the laser beam is adjusted by adjusting the beam spot size on the target.[165,166]

Park et al.[156] evaporated In_xSe (x∼1)/Cu_2Se double layers from In_2Se_3 and Cu_2Se sources on unheated substrates. The films were subsequently annealed in a Se atmosphere at 550°C

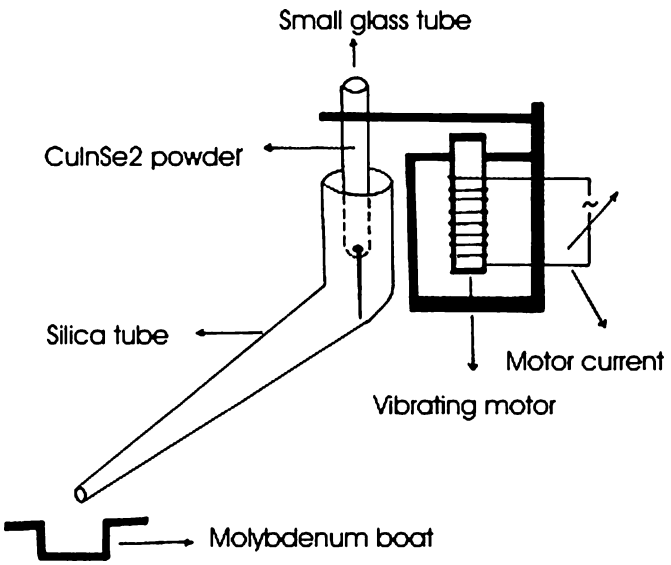

FIG. 12. A schematic view of a flash evaporation equipment. Reprinted from *Vacuum*, 61, Akl et al., Structural study of flash evaporated $CuInSe_2$ thin films, 75–84, © 2001 Elsevier, with permission from Elsevier.

to yield crystalline single-phase Cu- and Se-rich $CuInSe_2$ films. After annealing, small amounts of In_2Se_3 and Se were deposited on the film surface at the same temperature in order to form a thin $CuIn_3Se_5$ layer. A solar cell efficiency of 5.4% was achieved with a n-ZnO/i-ZnO/CdS/$CuIn_3Se_5$/$CuInSe_2$/Mo structure.[156] The efficiency increased to 9.6% when the process was slightly modified: Se was co-evaporated with In_2Se_3 during the initial stage at substrate temperature of 150°C, and during the Cu_2Se evaporation stage the substrate temperature was increased to 440°C which was also used for the subsequent Se annealing (10 min). The Cu-poor surface layer was formed again by evaporating small amounts of In_2Se_3 and Se.[157]

The sequential "quasi-flash evaporation" of In_2Se_3 and Cu_2Se onto unheated substrates and a subsequent anneal at 500°C under Ar for 1 h resulted in single-phase chalcopyrite CIS films with random orientation and p-type conductivity. The evaporation of In_2Se_3-Cu_2Se mixtures by the same method led to the formation of (112) oriented single-phase CIS after annealing at 400°C. The control of the film composition in the latter method was difficult, however, because In_2Se_3 melted earlier than Cu_2Se, and the evaporating In_2Se_3 vapor caused some loss of the unmelted Cu_2Se powder by splashing it off from the crucible. That is why the films evaporated from the mixture of In_2Se_3 and Cu_2Se were highly Cu-deficient and thus n-type.[158]

Thermal evaporation of p-type $CuInSe_2$ thin films from a single CIS source at substrate temperatures ranging from 200 to 600°C was reported by Sadigov et al.[127] Because of difficulties in achieving stoichiometric, crystalline, and binary phase free films with good surface morphology, additional Cu and In were evaporated on the films at room temperature, and the films were subsequently selenized in elemental Se vapor.[127] Yamaguchi et al.,[159] in turn, evaporated In and $CuInS_2$, and annealed the precursor stack in elemental S and Se atmospheres in a quartz tube. The S/(S+Se) ratio in the resulting film was found to depend on the S/(S+Se) ratio in the annealing atmosphere. In addition to (112) oriented chalcopyrite $CuIn(S,Se)_2$, the $CuIn_5S_8$ phase was also found in the films.[159]

Klenk et al. prepared CIS, CGS, and CIGS films from CIS and CGS powders and their mixtures at substrate temperatures between room temperature and 350°C both by thermal[105] and flash[160] evaporation. In both cases, the films were Se-deficient unless the evaporation was done in the presence of additional Se vapor.[105,160] The films were annealed in the presence of Se vapor at high temperatures of up to 550°C.[105,160] Thermal evaporation resulted in uniform and dense films when the substrate temperature was between 200 and 300°C; film thickness (1.5 μm) and composition were nearly constant over an area of 10 cm × 10 cm. Film formation was found to proceed via the binary selenides—probably because the relatively slow heating rate of the CIS and CGS precursor powders caused their decomposition. A significant difference between the formation kinetics of CIS and CGS was observed: the formation of single-phase $CuGaSe_2$ required reaction temperatures above 500°C, whereas single-phase chalcopyrite $CuInSe_2$ was obtained already at 350°C, with no significant improvement of crystallinity at higher temperatures. Moreover, single-phase CIGS was obtained only when the Ga content of the film was below 6 at.%.[105] Solar cell efficiencies above 10% were achieved with CIGS absorbers,[105] whereas the efficiencies with the ternary absorbers were lower, between 3–4% for CGS[105,160] and 6% for CIS.[105] Substrate temperature did not significantly affect the composition of flash evaporated films.[160]

Often, however, the compositions of flash evaporated films have been found to depend on substrate temperature. Merino et al.[161] studied the flash evaporation of CIS and CIGS from two types of crucibles at different substrate temperatures. About 10 wt% of Se powder was added to the crucible with the compound source in order to prevent the formation of Se-poor films. The deviations of the film stoichiometry from the source material were minimized by carefully choosing the temperatures of crucible and substrate and keeping the deposition rate low enough. Most films were n-type but became p-type after annealing in Se vapor. Solar cells with standard CdS and ZnO films were made by co-evaporating a thin $CuIn_2Se_{3.5}$ layer on the absorber. The best efficiencies were 5.1% for CIS and 6% for CIGS.[161]

Amorphous CIS films have been deposited by flash evaporation onto unheated substrates.[162,163] XRD reflections of CIS and Cu_7In_4 together with some unidentified peaks appeared when the substrate temperature was 200°C or above. Also post-deposition annealing at 350°C resulted in the formation of CIS, Cu_7In_4 and In_2Se_3. The optimum conditions for the formation of CIS were determined to be a substrate temperature of 250°C and post-deposition annealing at 350°C for 3–4 h.[163] On the other hand, Joseph and Menon[164] prepared crystalline p-type CIS films by flash evaporation from a single CIS source onto unheated substrates.

Victor et al.[165] prepared (112) oriented CIS thin films by PLD at a substrate temperature of 150°C. The chalcopyrite phase was present already in the as-deposited films, and the crystallinity was further increased by annealing in Ar at 500°C for 10 or 20 s. Kuranouchi et al.[166] deposited CIS films on unheated substrates and at a substrate temperature of 500°C. The films were post-annealed at 500°C in vacuum. The films deposited at room temperature exhibited (112) orientation after annealing.[166]

4.1.4 Chemical Vapor Deposition

Chemical vapor deposition (CVD) is a versatile thin film deposition method for a wide range of materials. CVD can also be scaled up to large area substrates as demonstrated by SnO_2 transparent conductor[96] and self-cleaning TiO_2 coating[97] depositions on-line in soda-lime glass float processes.

CIS thin films have been deposited by atmospheric pressure metal organic chemical vapor deposition (AP-MOCVD) using $Cu(hfac)_2$ complexed with trimethylamine $N(CH_3)_3$[167] and diethylamine $NH(C_2H_5)_2$[168] as the Cu precursors. Trimethylindium $In(CH_3)_3$ and triethylindium $In(C_2H_5)_3$ were used as the In precursors and H_2Se as the Se precursor. H_2 was used as the carrier gas. The depositions were carried out at 400°C, and the resulting

films exhibited strong (112) orientation regardless of the metal ratio.[167,168] Solar cells fabricated from the CVD-grown films were not very efficient; the maximum open circuit voltage was 0.26 V.[168] For comparison, the open circuit voltages of high-efficiency devices are generally above 0.6 V.[6,49–53]

A plasma-enhanced CVD process has also been reported[169] where hexafluoroacetylacetonate complexes $Cu(hfac)_2$ and $In(hfac)_3$ were used as the metal precursors and 4-methyl-1,2,3-selenadiazole as the Se source. H_2 was used as the carrier gas for the metal precursors. Deposition temperatures ranged from 150 to 400°C. The resulting films were Se deficient probably due to a Se loss during post-deposition cool-down in vacuum.[169]

O'Brien et al.[170–172] have deposited $CuInSe_2$, $CuInS_2$, and $CuGaS_2$ thin films by low-pressure MOCVD (LP-MOCVD)[170,171] and aerosol-assisted MOCVD (AA-MOCVD)[171,172] using dual-source precursors. The LP-MOCVD precursors for the $CuInSe_2$ films were methyl-*n*-hexyl-diselenocarbamate complexes of Cu(II) and In(III), that is, $Cu(Se_2CNCH_3C_6H_{13})_2$ and $In(Se_2CNCH_3C_6H_{13})_3$, respectively.[170,171] The $CuInSe_2$ films were deposited at 400–450°C while the precursors were kept at 180–250°C. The resulting films were polycrystalline, and their compositions were close to stoichiometric. The band gaps of the CIS films were estimated to be about 1.08 eV.

For aerosol-assisted MOCVD,[171,172] the precursors were dissolved in toluene or tetrahydrofuran. The aerosol was generated using an ultrasonic humidifier and transferred to the reactor by the carrier gas. In Ref. 171, the same precursors were used as in the LP-MOCVD studies, that is, $Cu(Se_2CNCH_3C_6H_{13})_2$ and $In(Se_2CNCH_3C_6H_{13})_3$. The substrate temperature was between 425 and 475°C, and according to XRD, the resulting films were chalcopyrite $CuInSe_2$. In Ref. 172, the AA-MOCVD precursors were iminobis(diisopropylphosphine selenide) complexes of Cu(II) and In(III), that is $\{Cu[SeP(CHCH_3CH_3)_2]_2N\}_3$ and $In\{[SeP(CHCH_3CH_3)_2]_2N\}_2Cl$, respectively. The deposition temperature was between 375 and 450°C. The resulting films had a favorable, slightly Cu-poor composition (Cu 23%, In 27%, Se 50%), and showed the characteristic XRD reflections of the chalcopyrite phase with a preferred (112) orientation.[172] In most cases, films deposited either by LP-MOCVD or by AA-MOCVD exhibited rough surface morphologies.[171,172] Only the films deposited by LP-MOCVD on ITO-glass and Si(100) substrates showed smoother surfaces with homogeneous particle sizes.[171]

In order to achieve even better control of the film composition than with the dual-source precursors described earlier, Banger et al.[173,174] have synthesized single-source precursors for a variety of ternary chalcopyrite compounds. Preliminary growth experiments with $(PPh_3)_2Cu(SeCH_3)_2In(SeCH_3)_2$ resulted in near stoichiometric, (112) oriented chalcopyrite $CuInSe_2$ films.[173]

4.1.5 Close-Spaced Vapor Transport

CIS,[175] CGS,[175] and CIGS[175,176] thin films have been deposited by close-spaced vapor transport using iodine as a transport agent.[175,176] The reactor, shown in Figure 13, is a vertical vacuum tube that contains the desired compound as a powder, a substrate, and solid iodine. The tube is heated, and the reaction starts when iodine vaporizes and reacts with the source powder to form gaseous metal iodides and Se_2. The gaseous species then react on the substrate surface, forming the desired compound and liberating iodine. Advantages of the method include low cost and the possibility to deposit films on large substrate areas. $CuIn_{1-x}Ga_xSe_2$ films with compositions identical to those of the source materials were obtained within the whole composition range (x from 0 to 1). Moreover, the films exhibited chalcopyrite structure, good surface morphology, and p-type conductivity.[175] The morphology of the deposit was found to depend on the grain size of the source powder: large-grained source powder resulted in a bilayer structure where the initial (lower) layer consisted of considerably smaller grains than the upper one. The formation of the small-grained initial layer could be prevented using smaller-grained source powder that resulted in the formation of large-grained, smooth films.[176]

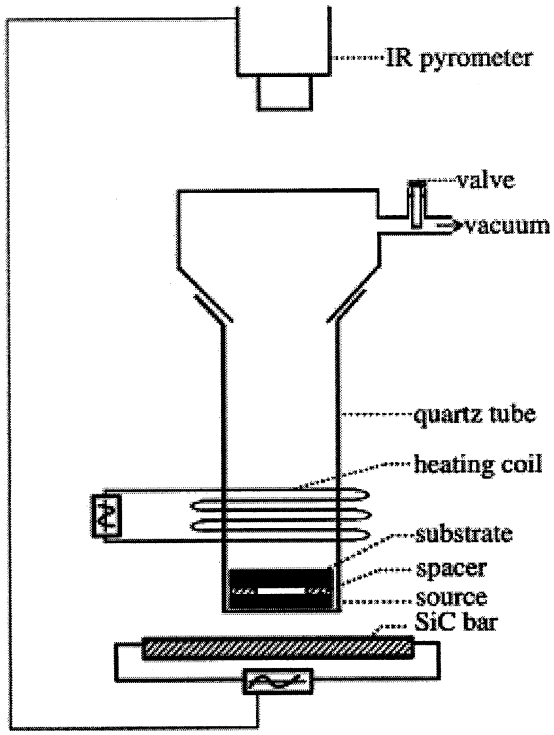

FIG. 13. A schematic view of a close-spaced vapor transport reactor. Reprinted from *Thin Solid Films*, 414, Massé et al., Morphology of $Cu(In,Ga)Se_2$ thin films grown by close-spaced vapor transport from sources with different grain sizes, 192–198, © 2002 Elsevier, with permission from Elsevier.

4.1.6 Spray Pyrolysis

Single-phase chalcopyrite CIS and CIGS thin films with strong (112) orientation and p-type conductivity have been

prepared by spray pyrolysis from acidic aqueous[177] and aqueous-ethanolic[178] solutions of $CuCl_2$, $InCl_3$, $GaCl_3$, and N,N-dimethylselenourea. The $[Cu^{2+}]/([In^{3+}] + [Ga^{3+}])$ concentration ratios in the solutions were kept at 1, but an excess of selenium precursor was needed in order to compensate for the Se loss during deposition.[177,178] Films deposited from aqueous solutions at substrate temperatures between 300 and 350°C were nearly stoichiometric.[177] Deposition temperatures lower than 275°C led to Cu-poor films, whereas Cu-rich films were obtained at temperatures higher than 350°C.[177] Oxygen was found in the as-deposited films, and the films deposited below 300°C contained also carbon and chlorine impurities.[177] Annealing in selenium atmosphere at 300°C for 30 min did not affect the elemental composition. On the other hand, annealing in vacuum at the same temperature and for the same duration decreased the selenium and indium contents, which was attributed to their re-evaporation from the film. Air-annealing at 300°C for 30 min led to the formation of oxides of In, Ga, and Se.[177] Films deposited from aqueous-ethanolic solutions[178] at 400°C were slightly (In+Ga)-rich, with a higher Ga/(In+Ga) ratio than in the deposition solution. At slightly lower substrate temperatures (360°C) the films were either Cu- or (In,Ga)-rich, depending on the In/Ga ratio in the deposition solution, and their Ga/(In+Ga) ratios were closer to those in the deposition solutions.[178] Despite these promising results, the solar cell efficiencies reached with spray-pyrolysed absorbers are low, about 4–5%.[177]

4.1.7 Electrodeposition

Electrochemical techniques for the preparation of CIS-based films include one-step deposition, sequential deposition of binary compounds, and deposition of elemental layers followed by annealing under either an inert or a reactive atmosphere. The latter approach was discussed in section 4.1.2., together with other two-stage deposition methods. This section focuses on one-step electrodeposition of $CuInSe_2$ thin films.

Figure 14 shows a three-electrode setup used commonly in electrodeposition. Two of the electrodes, that is, the working electrode and the counter electrode, are connected to the power source. The substrate is connected as the working electrode, and an inert electrode, often a Pt wire or plate, is used as the counter electrode. The third electrode, that is, the reference electrode, is needed in potentiostatic electrodeposition where the potential of the working electrode is controlled in a predetermined manner. The potentiostat measures and controls the potential of the working electrode with respect to the reference electrode. The aim is to minimize the difference between the measured and predetermined potentials, and this is attained by adjusting the current that flows between the working electrode and the counter electrode. The potential of the reference electrode must be known, and furthermore it must stay constant during the deposition. To satisfy the latter requirement, no current is allowed to flow through the reference electrode. Silver-silver chloride electrode (Ag/AgCl) and calomel electrode (Hg/Hg_2Cl_2) are examples of commonly used reference electrodes.

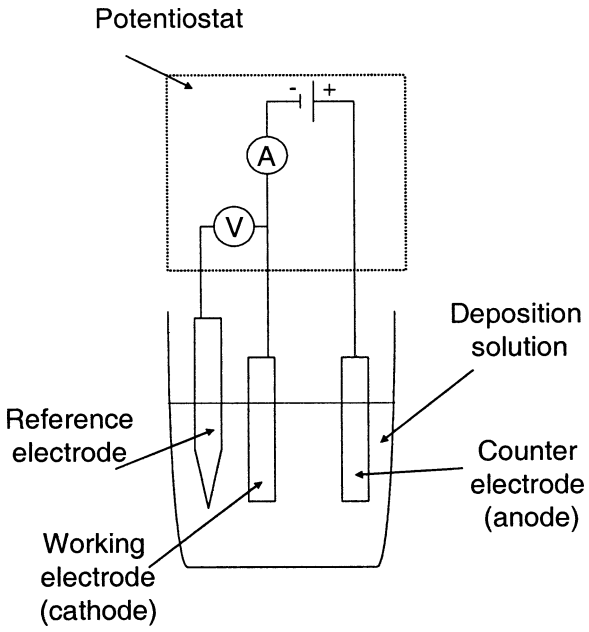

FIG. 14. A schematic view of the three-electrode setup used in cathodic electrodeposition.

Electrodeposition of CIS-based thin films has been studied extensively by several groups since 1983 when Bhattacharya[179] published the first paper on one-step electrodeposition of $CuInSe_2$ thin films. One-step electrodeposition of CIS is usually carried out potentiostatically at RT from aqueous solutions that contain simple compounds of Cu^{2+} or Cu^+ and In^{3+}, most often sulfates[124,180,181–191] or chlorides.[184,188,189,192–201] Galvanostatic[194,195,202] and pulsed electrodeposition[189,200,201] have been used as well. Because of the limited solubility of Cu^+ compounds and the instability of the free Cu^+ ions in aqueous solutions, Cu^{2+} compounds are used considerably more frequently than Cu^+ compounds. The most popular Se precursor is SeO_2, which dissolves into mildly acidic solutions in the form of $HSeO_3^-$,[203] but Na-selenosulfate[194] has been used as well. Acidic solutions are used because the reduction of $HSeO_3^-$ is facilitated in acidic solutions.[203]

The deposition solutions often contain a complexing agent in order to shift the reduction potentials of Cu and In closer together and/or to improve the film quality. The most popular complexing agent is citric acid[180–183,185,187,194,197,204] that acts also as a pH buffer, but other ligands such as ammonia,[179,194] triethanolamine,[179] ethylenediamine,[205] ethylenediaminetetraacetic acid (EDTA),[199] and thiocyanate[184,188,206,207] can be used too. Sometimes a supporting electrolyte such as sulfate (K_2SO_4)[180,181,190] or chloride (LiCl,[192,193] NaCl,[199] or KCl[208]) is added.

Electrodeposition of CIS thin films is usually carried out from solutions where the Cu and Se precursor concentrations are of the

same order of magnitude, and only the In precursor is sometimes present in excess. Under such conditions, film stoichiometry is determined by the deposition potential and the ratio of diffusion fluxes of Se and Cu to the substrate surface.[180,209] Balancing of fluxes can be done by careful optimization of the deposition conditions, that is, adjusting the concentrations in the solution as well as the deposition potential. The disadvantage of the flux balance approach is that the concentration and potential ranges for the formation of stoichiometric product are often narrow, and thus small, unavoidable variations in concentrations and potential may result in large changes in the film compositions. This deteriorates the reproducibility and may make upscaling to larger substrate areas problematic.

For comparison, CdTe, another important solar cell absorber, is usually electrodeposited utilizing induced co-deposition where the film composition is determined by thermodynamics.[210,211] The more noble element (Te) deposits first on the electrode surface, and induces the compound formation at less negative potentials than where the less noble element (Cd) would deposit alone. The reason for the underpotential reduction of the less noble ion is the energy released in the compound formation. When the concentrations in the deposition solution are chosen so that the solution contains a large, 10–100 fold, excess of the less noble ion, the deposition of stoichiometric CdTe is ensured over a range of electrolyte compositions and electrode potentials. This kind of induced co-deposition process, employed most widely for CdTe but also for many other binary compound semiconductors,[212–214] is much less sensitive to the unavoidable variations in the electrolyte compositions than processes that rely on balancing the diffusion fluxes. In addition, small potential drops across large substrates have minimal effects.

Main reason for the lack of CIS electrodeposition processes utilizing the induced co-deposition is that the electrodeposition of CIS occurs via the formation of copper selenide, which does not follow the induced co-deposition mechanism.[180,215] The complicated behavior of the Cu-Se system may be attributed to the following facts. First, the reduction of Se^{4+} to Se requires a large overpotential, that is, its actual reduction potential is much more negative than the corresponding standard reduction potential ($E^\circ = +0.556$ V vs. Ag/AgCl[203]), and this potential is also dependent on the electrode surface. Second, the standard reduction potentials of Cu^+ and Cu^{2+} ($E^\circ = +0.298$ V and $+0.115$ V vs. Ag/AgCl,[203] respectively) are close to the observed reduction potential of Se^{4+} and, depending on the required Se overpotential, may be either more positive or more negative than that of the Se^{4+} ions. Further complications may arise from the passivating nature of Se deposited at room temperature.[215] In some cases the reduction potential of Se^{4+} has been found to shift to the positive direction in the presence of Cu^{2+} in the solution.[180,215] In fact, Vedel et al.[180,215] observed the deposition of Se in reasonable quantities only in the presence of Cu^{2+} in which case the formation of copper selenide enabled the deposition of Se. Thus the Cu-Se system does not follow the induced co-deposition mechanism in the same way as the Cd-Te system does.[210,211]

The aforementioned complications can, however, be overcome, by shifting the reduction potential of the copper ion far enough to the negative direction so that Se deposits first.[206,216] In Ref. 206, suitable conditions for induced co-deposition were achieved by complexing the Cu^+ ions by thiocyanate ions (SCN^-) that form strong complexes with Cu^+ ions.[217,218] Due to the complexing, the reduction potentials of the Cu^+ ions shifted considerably to the negative direction, so that the deposition of metallic Cu did not start until at -0.75 V vs. Ag/AgCl.[206] Thus the negative potential shift with respect to the standard reduction potential of Cu^+ ($+0.298$ V vs. Ag/AgCl[203]) was more than 1 V. When compared to the reduction potential of Cu^+ ions in weak chloride complexes (-0.3 V vs. Ag/AgCl[206]), the shift was 0.45 V.[206] The reduction of Se^{4+} started at about -0.2 V vs. Ag/AgCl, and induced the formation of $Cu_{2-x}Se$ (with $x = 0.15$–0.5) between -0.25 and -0.65 V vs. Ag/AgCl, that is, at less negative potentials than where the deposition of metallic Cu started.

In contrast to the complicated behavior of Se in the presence of Cu, the behavior of the Cu-Se system in the presence of In^{3+} is analogous to that of Te in the presence of Cd^{2+}, that is, copper selenide induces the formation of CIS. In the presence of an excess of In^{3+} in the solution, the film composition is controlled by the Se^{4+}/Cu^{2+} flux ratio arriving at the electrode.[180] At low flux ratios, two co-deposition processes were observed, and the resulting films consisted of either CIS + Cu_2Se or CIS + Cu. If the Se^{4+} flux is in excess, the two processes merge and only CIS + In_2Se_3 are obtained.[180] When the In^{3+} concentration is not high enough, the electrodeposition process is limited by diffusion of all ions. Consequently, the film composition is determined by both Se^{4+}/Cu^{2+} and In^{3+}/Cu^{2+} flux ratios.[209]

CIS electrodeposition process controlled fully by the induced co-deposition mechanism could be developed by using the SCN^- complexed solution. As noted earlier, in this solution also the formation of $Cu_{2-x}Se$ occurred by the induced co-deposition mechanism. After adding In^{3+}, that is only weakly complexed by SCN^-, nearly stoichiometric CIS ($Cu_{1.30}In_{1.00}Se_{2.18}$ according to TOF-ERDA) was deposited at the same potential range where the $Cu_{2-x}Se$ formation occurred in the absence of In^{3+}, that is, between -0.25 and -0.65 V vs. Ag/AgCl.[206,207,219] The film composition also remained essentially constant when the concentration ratio of the Cu and In precursors was varied over a wide range of 0.1–2.5.[206]

Electrodeposited CIS and CIGS films are usually amorphous or poorly crystalline and consist of small grains in their as-deposited state. They tend to be Cu-rich and contain frequently degenerate $Cu_{2-x}Se$ phases that are detrimental to the device performance. The films may also contain impurities that originate from the aqueous deposition solution or from the complexing agents. For these reasons, the films require at least annealing under an inert atmosphere prior to completing the device. Often the film stoichiometry needs to be corrected too, for instance by

annealing under a Se-containing atmosphere and/or by selective etching in cyanide-containing solutions to remove the excess Cu and Se. Electrodeposited CIS and CIGS films can nevertheless be used as precursor layers for high-efficiency absorbers as will be described in section 4.1.8.

In spite of the large amount of literature on electrodeposited CIS thin films, only a few publications report solar cell results. The highest conversion efficiencies achieved by one-step electrodeposited $CuInSe_2$ absorber films without subsequent annealing under Se-containing atmospheres are those of Qiu and Shih.[202,220] Their CIS films were deposited from a single solution that contained "ions and complexes of Cu, In, and Se."[221] The films were post-deposition annealed at temperatures between 300 and 420°C for 20 min under Ar or in vacuum, and resulted in conversion efficiencies of 7%[202] with a Mo/CIS/CdS/CdS:In structure and in 6.3% with a Mo/CIS/CdS/ZnO structure.[220]

Guillemoles et al.[29] obtained a conversion efficiency of 6.5% using electrodeposited CIS films. The films were deposited according to Ref. 180 and post-deposition annealed under elemental Se atmosphere for 20–30 min at 400–450°C. The Cu/In ratio did not change upon annealing but the Se content increased, partly due to the formation of $MoSe_2$ between Mo and CIS. After annealing, the characteristic chalcopyrite XRD reflections were observed also for the In-rich films, and the films were also strongly (112) oriented. Cu-rich films had larger grain sizes and less preferential orientation.[29]

Kampmann et al.[190] electrodeposited $CuInSe_2$ films on large substrate areas (80 cm^2) from solutions containing 1.0 mM $CuSO_4$, 3.0 mM $In_2(SO_4)_3$ and 1.7 mM SeO_2 at pH 2.4. 0.3 M K_2SO_4 was used as the supporting electrolyte. The as-deposited films were selenized at 500°C under elemental selenium atmosphere, and resulted in a conversion efficiency of 4.8%.

Chaure et al.[191] reported a glass/SnO_2:F/n-CdS/n-CIS/i-CIS/p-CIS/Au structure where all the CIS films were prepared by electrodeposition from a single electrolyte containing 2.0 mM $CuSO_4$, 4.0 mM $In_2(SO_4)_3$ and 4 mM SeO_2 at pH about 2. The CIS films with different conductivity types were deposited at different potentials: n-type CIS at −1.0 V, i-type at −0.75 V, and p-type at −0.6 V vs. Ag/AgCl. The as-deposited structure was annealed at 450°C under a Se atmosphere and etched in a KCN solution. The V_{OC}, j_{SC}, and FF under AM1.5 conditions were 0.41 V, 36 mA/cm^2, and 0.45, respectively.[191] The conversion efficiency calculated from these values is 6.6%.

Sudo et al.[196] electrodeposited CIS films from uncomplexed chloride solutions and annealed them at 350°C under N_2 prior to device completion. A low conversion efficiency of 1.5% was obtained for a film with Cu/In ratio of 0.95.

A conversion efficiency of 1.3% was obtained for a cell with a CIS film prepared by the induced co-deposition from the SCN^- complexed solution. Prior to device completion, the film was first annealed at 400°C under N_2 and then etched in 0.5 M KCN to improve the film crystallinity and composition, respectively.[222] The CIS films prepared by the induced co-deposition were used in all-electrodeposited CIS/ZnO pn-junctions as well.[223] The electrodeposited junctions gave promising I-V characteristics in the dark.[223]

All-electrodeposited CIS/CdS pn-junctions of Raffaelle et al.[187] showed good I-V characteristics in the dark. The p-type CIS films were deposited from solutions containing 1 mM $CuSO_4$, 10 mM $In_2(SO_4)_3$, 5 mM SeO_2, and 25 mM Na-citrate.[187]

4.1.8 Low-Temperature Liquid Phase Methods for Precursor Deposition

CIS films prepared by non-vacuum methods such as electrodeposition, electroless deposition, and chemical bath deposition, can be used as precursors for high-efficiency absorbers. These are inherently low-cost methods because the deposition temperatures are generally low and the equipment is simple. Precursors prepared by these methods need usually at least a post-deposition treatment at high temperatures under selenium-containing atmospheres to obtain high-efficiency devices. It must be noted that especially electrodeposition of CIS-based materials has been studied extensively, and the process described here uses the electrodeposited film only as a precursor layer. The numerous other electrodeposition processes were described in detail in the previous section.

Bhattacharya et al. have studied extensively the preparation of CIGS solar cells from precursors prepared by electrodeposition,[192] electroless deposition,[193] and chemical bath deposition.[179,224] A feature common to all these non-vacuum processes is that the film stoichiometry has to be adjusted after deposition by adding In, Ga, and Se by physical vapor deposition at high substrate temperatures, usually at 550–560°C. Although this may be considered as a drawback, these are nevertheless promising methods for the preparation of precursor films.

The electrodeposited precursors were deposited at room temperature from acidic (pH about 2) aqueous solutions containing 0.02–0.05 M $CuCl_2$, 0.04–0.06 M $InCl_3$, 0.01–0.03 M H_2SeO_3, 0.08–0.1 M $GaCl_3$ and 0.7–1 M LiCl.[192,193] The deposition potential was −1.0 V vs. Pt, and the as-deposited films were highly Cu-rich with a composition of $CuIn_{0.32}Ga_{0.01}Se_{0.93}$. After the stoichiometry correction by PVD, the film composition had changed to $CuIn_{0.72}Ga_{0.47}Se_{2.05}$, and resulted in a solar cell efficiency of 15.4%.[192]

Electroless deposition is based on redox reactions without an external current source. Cu-rich Cu-In-Ga-Se films were prepared from aqueous solutions containing $CuCl_2$, $InCl_3$, H_2SeO_3, $GaCl_3$ and LiCl, using a Fe electrode as the reductant. After the stoichiometry correction by PVD, the films were completed to solar cells and a conversion efficiency of 13.4% was achieved.[193]

Chemical bath deposition is based on spontaneous but kinetically controlled precipitation reaction between the constituent ions. One of the advantages of the method is that the deposition equipment is very simple as illustrated in Figure 15. Chemical

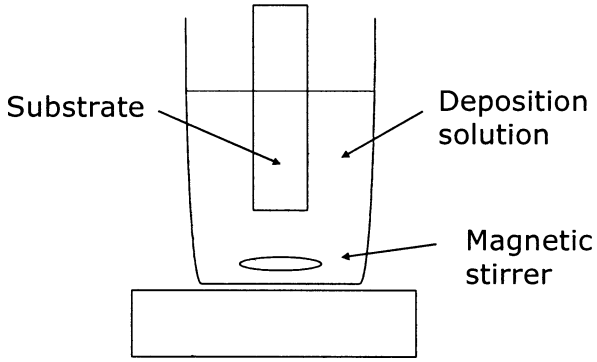

FIG. 15. A schematic view of a chemical bath deposition setup.

bath deposition is done most often in an aqueous solution. Precipitation occurs when the concentrations of the ions in the solution are high enough so that their ionic product exceeds the solubility product (K_s) of the compound to be deposited. Depending on the supersaturation ratio, that is, by how much the concentrations exceed the solubility product, the growth can be heterogeneous (film on a substrate) or homogeneous (precipitate in the solution). Heterogeneous growth dominates at low supersaturation.[225]

CIS[179,226] and CIGS[224] thin films have been prepared by chemical bath deposition using sodium selenosulfate (Na_2SeSO_3) as the selenium precursor. Garg et al.[226] deposited CIS films at 40°C using $Cu(NH_3)_4^{2+}$ and citrate-complexed In^{3+} ions as the metal precursors. After post-annealing at 520°C in air, V_{OC} about 0.3 V was measured for a n-Si/p-CIS heterojunction.[226] Bhattacharya[179] used triethanolamine complexes of $Cu^+$and In^{3+} as the metal precursors. Cu-rich CIGS precursor films were deposited from solutions containing $Cu(NO_3)_2$, $In(SO_3NH_2)_3$, $Ga(NO_3)_3$, Na_2SeSO_3, triethanolamine, NH_4OH and/or NaOH. After stoichiometry correction by PVD, the films were used as absorbers in solar cells that exhibited an efficiency of 7.3%.[224]

4.1.9 Chalcogenization of Particulate Precursor Layers

One group of techniques involve the deposition of particulate precursor materials onto substrates at low temperatures and subsequent sintering under a chalcogen atmosphere. The precursors are typically sub-micron powders of metals, alloys, oxides, or chalcogenides, and they are deposited as inks, suspensions, or pastes by simple techniques such as printing, casting, spraying, doctor-blading, spin-coating, or dip-coating. The porous precursor layer converts into a dense, large-grained film at the high (400°C or above) sintering temperature. An important advantage of these methods is that because the metal ratio is fixed already in the precursor material, the stoichiometry of the final film is independent of thickness. Consequently, compositionally uniform films can be prepared over large areas and relatively large thickness variations can be tolerated.[227,228] Cell efficiencies between about 10 and 13%,[227–230] submodule efficiencies between 7 and 8% (area 50–150 cm^2)[227] and module efficiency of 5%[228] have been achieved by the absorbers made with these techniques.

Norsworthy et al.[229] prepared a metallic powder containing Cu-In alloys, spread the powder over a substrate as an ink, and selenized the precursor layer under 5% H_2Se/N_2 at 440°C for 30 min to form CIS. Solar cells prepared using the ink-coated absorber exhibited efficiencies of 10–11%.[229] Another approach of the same group[230] involved dispersion of nanoparticulate mixed oxides of Cu, In, and Ga in water, and printing of this ink on a substrate. The oxides were converted to CIGS in two stages: first, the oxides were reduced to a Cu-In-Ga alloy under a H_2/N_2 atmosphere at 500–550°C. In the second stage, the alloy film was selenized in a H_2Se/N_2 mixture at 420–450°C. The conversion efficiency of a cell prepared on a flexible Mo foil was 10.1%.[230]

Kaelin et al.[231] compared the selenization of oxide, selenide, and metal particle precursors in Se vapor. Only the metallic precursor layers resulted in large-grained and dense CIS films. An In_2O_3 impurity phase was formed during the non-vacuum deposition of the metal precursor layers. Many of the selenized metal precursor films still contained In_2O_3 as an impurity phase that was attributed to the insufficient Se pressure during the selenization.[231]

4.2 Buffer Layer

As seen in Figure 3, most high-efficiency CIGS solar cells have a thin (50 nm or less) CdS buffer layer and an undoped ZnO layer between the absorber and the transparent conducting oxide. The roles of CdS and undoped ZnO are related to some extent.[232] Although the open circuit voltages of high-efficiency CIGS devices are mostly determined by the electric quality of the bulk absorber material,[58,59] the cell performances are nevertheless heavily influenced by the formation of the ZnO/CdS/CIGS heterojunction.[232] The role of the CdS buffer layer is twofold: it both affects the electrical properties of the junction and protects the junction against chemical reactions and mechanical damage. From the electric point of view, the CdS layer optimizes the band alignment of the device[27,233] and builds a sufficiently wide depletion layer that minimizes tunneling and establishes a higher contact potential that allows higher open circuit voltage values.[233] The buffer layer plays also a very important role as a "mechanical buffer" because it protects the junction electrically and mechanically against the damage that may otherwise be caused by the oxide deposition (especially by sputtering, see section 4.3). Moreover, in large-area devices the electric quality of the CIGS film is not necessarily the same over the entire area, and recombination may be enhanced at grain boundaries or by local shunts. Together with the undoped ZnO layer, CdS enables self-limitation of electric losses by preventing defective parts of the CIGS film from dominating the open circuit voltage of the entire device.[232]

The thickness as well as the deposition method of the CdS layer have a large impact on device performance. During the

early days, the device structures consisted of a $CuInSe_2$/CdS junction with a thick (about 1–3 μm) CdS layer.[194,195,221] The CdS layers of these devices were most often prepared by evaporation at substrate temperatures between RT and about 200°C, or in some cases by sputtering,[221] and the CdS film was often doped with either In[221] or Ga.[77] In some cases, a CdS bilayer was used,[139,202] consisting of a thinner high-resistivity layer, prepared either by evaporation[139] or chemical bath deposition[76,139,202] and a thicker low-resistivity layer, doped with 2% In[202] or Ga.[76] Evaporated CdS has been used also in combination with the transparent conducting oxide layer.[16,39,196] Nowadays chemical bath deposition (CBD) is used almost exclusively,[9,18] and therefore the next chapter focuses mainly on the effects caused by CBD-CdS.

4.2.1 Chemical Bath Deposition of CdS

As mentioned in section 4.1.8., CBD is a liquid phase deposition method that is based on a spontaneous but kinetically controlled reaction between the constituent ions. Film growth occurs when the concentrations of the ions in the solution are high enough so that their ionic product exceeds the solubility product (K_s) of the compound to be deposited, but low enough to prevent excessive precipitation in the solution.[225]

Commonly used Cd-precursors include simple compounds as $CdSO_4$,[52,233] CdI_2,[32,234] $Cd(CH_3COO)_2$,[78,232] and $CdCl_2$.[220] In order to slow down the reaction and to avoid the formation of $Cd(OH)_2$, the metal ion is usually heavily complexed by a ligand,[234] most often by NH_3.[32,52,78,220,232–234]

The most common sulfur precursor is thiourea NH_2CSNH_2,[32,52,78,220,232–234] the concentration of which is usually much higher than that of the metal precursor. The deposition is usually performed at an elevated temperature where thiourea hydrolyzes and decomposes releasing S^{2-} ions. The net reaction for the formation of CdS is

$$[Cd(NH_3)_4]^{2+} + NH_2CSNH_2 + 2OH^- \rightarrow CdS + 4NH_3 + CH_2N_2 + 2H_2O \quad [3]$$

After immersing the substrates in the deposition solution at room temperature, the bath is heated to the desired temperature that is usually between 55 and 90°C.[32,52,220,233,234] Deposition temperature influences strongly the film morphology and impurity content.[233]

In contrast to evaporated films,[235] CBD films contain high amounts of oxygen-related impurities that originate from the deposition solution; the amount of oxygen in the films can be as high as 10–15 at.%.[32,235] Most of the oxygen is present as OH^- and H_2O.[32,235] Thus, the composition of the CBD-CdS films is more accurately stated as Cd(S,O,OH).[32] Additional impurities such as C and N containing compounds result from the side reactions of thiourea.[235] The amount and identity of the impurities, and consequently the performance of the solar cell depend strongly on the CdS deposition conditions.[233,234,236,237] Negami et al.,[50] for instance, reported an increase of conversion efficiency from 17.6 to 18.5% when the CBD-CdS process was improved.

In addition to the CdS film deposition, the chemical bath also modifies the absorber surface. The bath has been suggested to re-establish positively charged surface states and the surface inversion by removing O_{Se} acceptors and creating Cd_{Cu} donors at the surface region.[18,100] Thus the interface between CIGS and CBD-CdS is not abrupt but the layers are intermixed to some extent.[31,32] Both Cu- and Cd-diffusion play a role, and the intermixing is further enhanced during the post-deposition air-annealing.[232] According to Nakada and Kunioka,[32] Cu is substituted by Cd at the surface region of CIGS. The diffusion depth of Cd atoms was about 10 nm, which may be related to the thickness of the Cu-deficient surface layer ($CuIn_3Se_5$) of CIGS.[32] On the other hand, Heske et al.[31] observed diffusion of Se and In from CIGS into CdS and the diffusion of S from CdS into CIGS. The extent of interdiffusion depends on the structure of the absorber: (220/204) oriented CIGS films have been found to allow more Cd atoms to diffuse into the CIGS film.[52]

One advantage of the CBD method as compared to evaporation is that a complete, conformal coverage of the CIGS surface can be obtained at very low thicknesses: already 10 nm has been reported to be sufficient.[238] The coverage depends on deposition conditions, particularly on the concentration ratio of the S and Cd precursors, being better with higher S/Cd precursor ratios.[236]

4.2.2 Interface Formation without Buffer Deposition

Absorption of light in the CdS layer, the band gap of which is 2.4 eV,[239] decreases the short circuit current density. Absorption of light in ZnO, in turn, is a less severe problem because its band gap is higher, 3.2 eV.[239] Therefore a thinner CdS layer results in a better device performance due to a reduced absorption of light.[76,77] The CdS layer must, however, be thick enough to obtain high open circuit voltage and fill factor.[233] If the CdS layer is too thin or does not exist at all, recombination in the space-charge region of CIGS increases, causing losses in V_{OC}, FF and spectral response.[233] Although the spectral response at short wavelengths (<550 nm) is enhanced in buffer-free devices, the response at the longer wavelengths is poor,[49] and consequently the conversion efficiencies are lower than those of the standard devices. For instance, similar absorbers resulted in conversion efficiencies of 18.8% and 15% with and without CdS, respectively.[49] Thus the optimum thickness of the CdS layer is a result of a compromise between increase in V_{OC} and FF, and loss in j_{SC}.[233]

Performances of buffer-free devices have been found to improve upon dipping the absorbers in solutions containing only $CdSO_4$ and ammonia but no thiourea at 60–80°C before the deposition of the transparent conductor.[233,240,241] Further improvement was observed upon applying a cathodic potential during the dip: Lincot et al.[240] achieved efficiencies of 11.3% and 9.4% with and without an applied potential during the dip, respectively. For comparison, an efficiency of 14.9% was measured for a device with the standard CdS and 5.9% for a buffer-free device without the $CdSO_4$-ammonia treatment.[240] These results support the idea

of Cd incorporation and doping of CIGS.[233] $CdSO_4$-ammonia treatments in combination with a very thin CdS film provided enhanced spectral response at short wavelengths[233] as compared to a high-efficiency device with the standard CdS. Because the j_{SC} values of the modified devices were slightly higher and the V_{OC} and FF similar to the high-efficiency devices with the standard CdS, this approach may result in improved cell performances.[233]

4.2.3 Chemical Bath Deposition of Zn-Based Buffer Layers

In order to decrease the optical absorption losses and to enhance the response in the short-wavelength region, alternative, more transparent buffer materials have been looked for. For instance, part of the Cd can be replaced by Zn to form (Cd,Zn)S, the band gap of which is higher than that of CdS.[106,239,242] Devaney et al.[106] deposited conformal, uniform (Cd,Zn)S buffer layers by CBD from $ZnCl_2$, $CdCl_2$, NH_4Cl, NH_4OH and thiourea at 85°C. The Zn content was varied, and the Zn/(Zn + Cd) ratio in the best films was 15–20%, resulting in a conversion efficiency of 12.5% with absorbers prepared by co-evaporation.[106] Başol et al.,[242] in turn, prepared (Cd,Zn)S buffer layers with about 10% Zn by CBD from Zn-acetate, Cd-acetate, triethanolamine, NH_4OH, and thiourea at 55°C, and achieved conversion efficiencies between 10 and 13% with absorber films prepared by particle deposition and subsequent selenization.[227,229]

Due to the environmental concerns associated with Cd-containing materials, serious efforts have been directed toward completely Cd-free buffer materials. The materials studied include Zn- and In-based materials such as sulfides, selenides, hydroxysulfides, and -selenides that can be prepared by CBD,[53,150,243–245] ion layer gas reaction (ILGAR),[246] MOCVD,[247] atomic layer deposition (ALD),[248,249] evaporation[43,250–254] and sputtering.[55] Analogously to the Cd-pretreatments described earlier, Zn- and In-pretreatments have led to improved device performances as well, either with or without an additional buffer layer.[193,240,246,248,255]

The conversion efficiencies of Cd-free devices are approaching those of the standard devices. Recently, a conversion efficiency of 18.1%, close to those of the best CdS containing devices, was achieved using a CBD-ZnS buffer layer in combination with a CIGS absorber prepared by three-stage co-evaporation.[53] ZnS layer was deposited by CBD from $ZnSO_4$, NH_3 and thiourea at 80°C.[53] It contained a significant amount of $Zn(OH)_2$ and ZnO phases and C and S impurities.[256] The band gap of the layer was, however, close to that of ZnS, 3.8 eV. When the structure was annealed in air at 200°C for 10 min,[53] the O-related impurities were not affected as studied by XPS but the cell performance improved markedly.[256] The improvement was probably due to diffusion of Zn into CIGS and formation of a buried pn-homojunction on the absorber surface. This intermixing explains why the conversion efficiency is surprisingly high in spite of the large conduction band offset between CIGS and ZnS.[53,152,256]

The diffusion of evaporated Zn into CIGS has also been observed.[255] The Zn-doping was accomplished by evaporating Zn on the heated CIGS surface either during or after the last stage of the three-stage co-evaporation process. Electron beam–induced current measurements revealed that the pn-junction of the device with Zn-doped absorber was located in CIGS, whereas in devices with CdS and ZnO buffers the junction was closer to the interface. The buffer-free solar cell with Zn-doped CIGS absorber gave a conversion efficiency of 11.5%.[255]

One of the Cd-free approaches of NREL[193]involved a Zn-diffused homojunction as well. The absorber was dipped in a $ZnCl_2$ solution and annealed at 200°C in air. Next the $ZnCl_2$ residue was removed from the absorber surface by washing in water and etching in concentrated HCl, followed by deposition of the ZnO bilayer by sputtering. The conversion efficiency of this device was 14.2%.[193]

The CBD-ZnS was found to be sensitive to oxygen-induced damage during sputter deposition of undoped ZnO, and thus the device was prepared without the undoped ZnO layer, that is, by depositing the conductive ZnO:Al layer directly on the ZnS by sputtering.[53] Sputter deposition of the conductive ZnO layer causes less damage to the underlying layer because it is done in Ar ambient without O_2 (see section 4.3). The optimum thickness of the ZnS layer was 130 nm.[53] As expected on the basis of the higher band gap of the buffer, the cell exhibited higher quantum efficiency at short wavelengths than a CdS-containing cell.[53,256] This resulted in a higher j_{SC} but V_{OC} was lower, resulting in a similar conversion efficiency as the standard cell with CdS.[53]

Showa Shell[150,151] likewise uses a ZnS-based CBD-buffer for their absorbers prepared by selenization of sputtered metal layers. A $Zn(OH,S)_x$ film is deposited from a solution containing Zn-sulfate or acetate, NH_3, and thiourea at a temperature above 80°C, followed by annealing of the CIGS/buffer structure at 200°C for 15 min in air, resulting in a buffer layer with a composition of $Zn(O,S,OH)_x$ (oxyhydroxysulfide).[243] Again, gain at shorter wavelengths and loss at longer wavelengths was observed as compared to CdS. The $Zn(O,S,OH)_x$ buffer suffered from sputter-induced damage during the ZnO deposition too, indicating the need for optimization of buffer thickness (currently 50 nm) and the ZnO deposition method.[243] Light soaking caused a remarkable improvement of the cell performance,[150,243] which was attributed to the release of H_2O molecules from the hydroxide during light soaking.[257] The efficiency of 12.5% for a 30 cm × 30 cm module[151] demonstrates the suitability of this $Zn(O,S,OH)_x$ buffer process to large substrate areas.

Kushiya et al.[243] studied also CBD-$Zn(O,OH)_x$ as buffer layers. The films were prepared by depositing $Zn(OH)_2$ at 60–80°C from similar solutions as $Zn(OH,S)_x$ but without thiourea, and by annealing to yield $Zn(O,OH)_x$. The improved performance after annealing was attributed to a conversion of hydroxide to oxide,[243] and not to Zn diffusion as was explained by Nakada and Mizutani.[256] Light soaking was again found to improve the cell performance.[243]

Ennaoui et al.[244] deposited Zn(S,OH) and Zn(Se,OH) buffer layers on CIGSS absorbers of Siemens by CBD at 50 and 70°C,

respectively. The deposition solutions contained $ZnSO_4$, hydrazine hydrate, NH_3, and thiourea or selenourea. The buffer deposition process was somewhat different from those mentioned earlier because it involved a Zn pretreatment: the absorbers were first dipped for a few minutes into the heated solution that contained the zinc precursor and the ligands, and the chalcogenide precursor solution was added only thereafter. The growth mechanism was self-limiting, allowing the deposition of very thin buffer layers with homogeneous surface coverages.[244] This approach led to total area efficiencies of 14.2% with both Zn(S,OH) and Zn(Se,OH) buffer layers.[244] Minimodule efficiencies (aperture area 20 cm^2) achieved by Zn(Se,OH) were between 10.7 and 11.7%, comparable to those achieved by the standard CdS buffer (11.7–12.7%).[244]

4.2.4 Chemical Bath Deposition of In-Based Buffer Layers

The use of indium-based buffer materials has resulted in high conversion efficiencies, too. Hariskos et al.,[245] for instance, deposited $In_x(OH,S)_y$ films on co-evaporated CIGS absorbers by CBD from $InCl_3$ and CH_3CSNH_2 (thioacetamide) at 70°C. Post-anneal at 200°C and light soaking resulted in an active area efficiency of 15.7%. Compared to the standard CdS buffer, the $In_x(OH,S)_y$ buffer resulted in improved V_{OC}, comparable FF, and slightly reduced j_{sc} values. Again, gain in short-wavelength region and loss in long-wavelength region was observed. The former was due to the improved transparency of the buffer layer, and the latter due to the modification of the electric properties of the absorber such as a reduced space-charge width.[245]

4.2.5 Alternative Methods for Buffer Deposition

Despite the aforementioned benefits, the CBD method has three disadvantages: first, the materials yield is low, which causes large volumes of Cd-containing waste. This problem can be partially solved by recycling the deposition solution: the CdS-containing colloidal material is filtered off after deposition, the concentrations of the Cd-precursor, NH_3 and thiourea are readjusted to the initial level. The properties of the CdS layers deposited from the recycled solution do not differ significantly from those deposited from the fresh solutions.[259] The second problem is the difficulty of combining the CBD step as a part of an in-line vacuum process: if both the absorber and the ZnO bilayers are prepared by PVD methods in vacuum, the CBD step causes an undesirable interruption of the vacuum process. Thirdly, the growth mechanism and the deposition rate, and thus the resulting film quality, depend strongly on the deposition conditions, that is, temperature, precursor concentrations, pH, and so on.[225] Therefore reproducibility may sometimes be a problem in CBD.

Recently, a new deposition method called ion layer gas reaction (ILGAR) was developed for the deposition of buffer layers.[246] It is a cyclic method that consists of application of a metal precursor on a substrate by dipping or spraying, drying the substrate, and the reaction of the metal precursor layer with gaseous hydrogen chalcogenide or water to form the corresponding metal chalcogenide or oxide. An evident advantage of ILGAR is that it produces less waste than CBD. The resulting films are conformal, and the film thickness is easily controlled by the number of deposition cycles.[241,246] The application of a ILGAR-ZnS buffer to Siemens absorbers resulted in total area conversion efficiency of 14.2% when a Zn-pretreatment in a $ZnCl_2$-NH_3 solution was performed before the deposition of the ILGAR-ZnS.[246]

To avoid the second problem of CBD, that is, its incompatibility with PVD processes, "dry," potentially more easily integrated, gas phase methods have been studied for buffer deposition. Siebentritt et al.,[247] for instance, deposited ZnSe buffer layers on Siemens CIGSS absorbers by photoassisted MOCVD using ditertiarybutylselenide as the selenium source and dimethylzinc or its adduct with triethylamine as the zinc source. Hydrogen was used as the carrier gas, and UV illumination was applied in order to enhance the decomposition of the Zn-precursor at low deposition temperatures. The highest total area efficiency, 11%, was achieved with a 10 nm thick buffer layer deposited at 280°C. This efficiency is the highest ever achieved with a MOCVD buffer.[247]

Lincot et al.[248,249] deposited Zn(O,S), In_2Se_3 and Al_2O_3 buffer layers by ALD. Diethylzinc, indium acetylacetonate, and trimethylaluminum were used as the metal precursors, water as the oxygen and H_2S as the sulfur precursor. Efficiencies of 10.4% for $ZnO_{0.85}S_{0.15}$, 13.5% for In_2Se_3, and 9% for Al_2O_3 were achieved. Further optimization of the In_2Se_3 process led to a conversion efficiency of 16.4%,[260] which was higher than that achieved with a standard CdS buffer (13.6%). This improvement was attributed to an unexpectedly high apparent band gap (2.7–2.8 eV) of the In_2Se_3 layer that enabled a better transparency and thus a higher short-circuit current.[260]

Konagai et al. used co-evaporation to prepare ZnSe[250] and $ZnIn_xSe_y$[251] buffer layers. The best conversion efficiencies achieved by these buffers were 9.1% and 15.1%, respectively, whereas the standard CdS resulted in 15.9%.[251] ZnSe buffers prepared by pulsed MBE gave a conversion efficiency of 11.6% after light soaking.[250] With In_2Se_3 (or In_xSe_y) buffer layers prepared by co-evaporation, conversion efficiencies of 8.5% on CIS[43] and 13% on CIGS[252] were obtained, whereas $(In,Ga)_ySe$ buffer layers prepared by the same method led to a conversion efficiency of almost 11%.[253].

Delahoy et al.[254] prepared $ZnIn_2Se_4$ (ZIS) and $ZnGa_xSe_y$ (ZGS) by evaporation of bulk material. The best efficiency achieved by ZIS was 11.6%, and no light soaking effect was observed. For comparison, the standard CdS buffer resulted in an efficiency of 16.3%, whereas 10.3% was measured for a buffer-free device.[254]

4.3 Transparent Conducting Oxide

There are two main requirements for the electric front contact of a CIGS device: sufficient transparency in order to let enough light through to the underlying parts of the device, and

sufficient conductivity to be able to transport the photogenerated current to the external circuit without too much resistance losses. Nowadays, transparent conducting metal oxides (TCO) are used almost exclusively as the top contacts. Narrow lined metal grids (Ni-Al) are usually deposited on top of the TCO in order to reduce the series resistance. The quality of the front contact is thus a function of the sheet resistance, absorption, and reflection of the TCO as well as the spacing of the metal grids.[106]

Referring to Figure 3, most devices utilize nowadays an oxide bilayer that usually consists of a thin (50–100 nm) high-resistivity layer, and a thicker (100–1500 nm) low-resistivity layer. The high-resistivity layer is most often undoped ZnO. Its benefit to the device performance is the increase of the V_{OC} by 20–40 mV.[232] The role of the high-resistivity layer is not completely understood yet, however. As discussed in section 4.2., the resistive oxide layer provides, together with the buffer, a series resistance that protects the device from local electric losses that may originate from inhomogeneities of the absorber.[232] Admittance spectroscopy and capacitance-voltage measurements[232] indicated that the presence of this resistive layer affects the electric properties of the heterojunction only to the extent that is expected on the basis of band diagrams. The conducting part of the oxide bilayer is most often ZnO doped with either Al,[49,51,62,76,78,105,115,152,228,247] B,[51,52,146,242,255,261] or Ga.[150,244,262] Also tin doped In_2O_3 (In_2O_3:Sn, ITO)[43,50,114] is commonly used.

4.3.1 Sputtering

The oxide bilayer is most often deposited by sputtering[43,49–51,62,76,78,105,115,117,150,152,228,244,247,262] with no intentional heating of the substrate.[51,62,76,262] The resistive layer is sputtered in Ar/O_2 (about 0.1–2%) ambient.[60,62,76,106] In addition to sputtering a pure ZnO target, the resistive layer may also be made from a doped target (ZnO:2 wt.% Al_2O_3),[60,76,106] provided that the sputtering ambient contains enough oxygen. Oxygen is needed to prevent the formation of oxygen vacancies that might render even the undoped ZnO too conductive. On the other hand, oxygen in the plasma also tends to cause damage to the underlying layers.[53,243]

The conductive layer (most often ZnO:Al) is usually deposited from a ZnO:2 wt.% Al_2O_3 target in a pure Ar ambient.[51,62,76,106] In some cases the sputtering ambient may contain a small amount of O_2.[60] The ZnO:Ga layers of Showa[262] and HMI[244] were sputtered in Ar from ZnO:Ga_2O_3 targets with Ga_2O_3 contents of 3.4 wt.%[262] or 5.7 wt.%.[244] Doping of the oxide layer can be accomplished also by reactive sputtering as was done for instance by Hagiwara et al.[51] who sputtered their ZnO:B electrodes from an undoped ZnO target in B_2H_6/Ar mixture.

4.3.2 Alternative Deposition Methods

Although sputtering is a fast and well-known deposition method for oxide thin films, its disadvantage is that it may damage the underlying layers.[53,243] Damage occurs especially during the deposition of the resistive layer that is done in the Ar/O_2 ambient. Nakada et al.,[53] for instance, had to leave the resistive ZnO layer out and to deposit a thicker ZnS buffer instead.

In order to reduce the damage caused by the oxide deposition, softer, less damaging deposition methods have been studied. The most important of these are MOCVD[118,146,242,255,261,263] and ALD[240,248,249,264] because they can be used for the deposition of the whole bilayer. In some cases only the resistive part of the oxide bilayer is deposited by a softer method, for instance MOCVD,[265] ALD,[263] ILGAR,[241] CBD,[243] or electrodeposition[258] and the conductive part by sputtering.

The less damaging oxide deposition methods are especially useful for the preparation of buffer-free devices where the protecting interlayer is absent. These buffer-free approaches have shown promising results: a conversion efficiency of 12.7% was measured for a device where the resistive ZnO layer was prepared by MOCVD and the conductive layer by sputtering.[265] For comparison, a device with MOCVD-ZnO bilayer showed an efficiency of 11.5%.[255] ALD-ZnO bilayers have resulted in even higher efficiencies, up to 14.9% with Cd pretreatment.[240] The combination of the two methods has also proven to be successful: a conversion efficiency of 12.1% was measured for a device with ALD-grown resistive ZnO layer and MOCVD-grown conductive layer.[263]

Bär et al.[241] measured a total area efficiency of 14.6% for a device where a part of the ZnO layer was deposited by ILGAR and the rest by sputtering. Solar cell preparation involved a pretreatment in an aqueous $CdSO_4$–NH_3 solution. The success of the ILGAR method was demonstrated by the somewhat higher efficiency than for the standard device, 14.1%.[241] Gal et al.[258] measured a conversion efficiency of 11.4% for a device with electrodeposited resistive ZnO layer and sputtered conductive ZnO layer. For comparison, the efficiency of a standard device with CBD-CdS and sputtered ZnO bilayer was 13.3%.[258] In Ref. 223, the entire oxide bilayer was prepared by electrodeposition. A good diode behavior was observed in the dark, but the resulting short-circuit currents were poor, most probably because the low conductivity of the electrodeposited films forced the illumination to be done through a thin Al contact layer.[223]

5. SUMMARY

$CuInSe_2$ and related chalcopyrite compounds are the most promising absorber materials for polycrystalline thin film solar cells. Cu(In,Ga)Se_2 solar cells have shown the highest conversion efficiencies of all thin film solar cells. The record efficiency is 19.2%, and several groups have achieved efficiencies over 18%. Further, the operational lifetimes of this type of solar cells are long due to their extraordinary stability.

$CuInSe_2$ thin films can be prepared from both gas and liquid phases by a variety of physical and chemical deposition methods, including evaporation from elemental or compound sources, selenization of precursor layers, chemical vapor deposition,

close-spaced vapor transport, spray pyrolysis, as well as low-temperature methods such as electrodeposition. The highest small-area efficiencies have so far been obtained by absorbers prepared by co-evaporation from elemental sources. As compared to evaporation, selenization of metallic precursor layers may offer an easier way to compositional uniformity over large areas; large-area absorbers prepared by selenization of metallic precursor layers have shown relatively high efficiencies (12–13%). Another advantage of this method is that it may lead to lower production costs of photovoltaic modules than evaporation. Other low-cost deposition methods are being developed as well. For example, absorbers prepared by selenization of particulate precursor layers, a relatively new method, have shown large-area efficiencies between 5 and 8%. Another interesting two-step approach is to deposit a precursor film by a low-temperature method such as electrodeposition, electroless deposition, or chemical bath deposition, and then correct the stoichiometry by adding In, Ga, and Se by physical vapor deposition methods. On the other hand, the physical vapor deposition step may be argued to increase the process cost beyond the low-cost limits. Absorbers prepared by either electroless deposition or CBD have not shown high efficiencies without the stoichiometry correction. Electrodeposited absorbers, instead, have shown more encouraging results.

The production costs can be lowered also by decreasing the absorber deposition time. Absorbers grown by fast co-evaporation have shown competent results, especially with reduced absorber thicknesses. The reduced thickness is an additional advantage because it reduces the amount of starting materials needed, and therefore lowers the costs further.

There is probably room for different deposition processes for different applications, that is, higher cost methods may be used in high-value applications like in satellites, where high efficiency is crucial, whereas less expensive methods may be needed to achieve low prices for mass products. The latter may become more important when photovoltaics become more and more common means of energy production.

An issue that has been subject to a lot of research is the replacement or even exclusion of the CdS buffer layer. Much progress has been made on that field and nowadays alternative buffer materials show performances that are almost comparable to CdS. Zinc-based and indium-based buffer materials have shown good performances in small-area solar cells; so have zinc-based materials on large areas.

Some of the alternative buffer materials are sensitive to the sputtering process commonly used for the deposition of the resistive part of the ZnO bilayer. Therefore, and also in order to enable the complete exclusion of the buffer layer, softer deposition methods have been developed for the resistive ZnO layer. These include metal organic chemical vapor deposition (MOCVD), atomic layer deposition (ALD), ion layer gas reaction (ILGAR), chemical bath deposition, and electrodeposition. Particularly the ILGAR method has given promising results. On the other hand, MOCVD and ALD have the advantage that they can be used for the deposition of the conductive part of the bilayer as well.

REFERENCES

1. T. Suntola, in *Proceedings of the PV CON '95*, Kruger, South Africa (1995).
2. L. D. Partain, Ed., *Solar Cells and Their Applications*, John Wiley & Sons, Inc., N.Y. (1995).
3. A. S. Bahaj, *Renew. Energy* **27**, 97 (2002).
4. J. L. Stone, *Phys. Today* **22**, September 1993.
5. M. A. Green, *Sol. Energy* **76**, 3 (2004).
6. K. Ramanathan, M. A. Contreras, C. L. Perkins, S. Asher, F. S. Hasoon, J. Keane, D. Young, M. Romero, W. Metzger, R. Noufi, J. Ward, and A. Duda, *Prog. Photovolt: Res. Appl.* **11**, 225 (2003).
7. H. Tsubomura and H. Kobayashi, *Crit. Rev. Solid State Mater. Sci.* **18**, 261 (1993).
8. A. Goetzberger, C. Hebling, and H. W. Schock, *Mater. Sci. Eng. R.* **40**, 1 (2003).
9. R. W. Birkmire and E. Eser, *Annu. Rev. Mater. Sci.* **27**, 625 (1997).
10. A. Goetzberger, J. Luther, and G. Willeke, *Sol. Energy Mater. Sol. Cells* **74**, 1 (2002).
11. R. W. Birkmire, *Sol. Energy Mater. Sol. Cells* **65**, 17 (2001).
12. A. Goetzberger and C. Hebling, *Sol. Energy Mater. Sol. Cells* **62**, 1 (2000).
13. A. Shah, P. Torres, R. Tscharner, N. Wyrsch, and H. Keppner, *Science* **285**, 692 (1999).
14. J. F. Guillemoles, L. Kronik, D. Cahen, U. Rau, A. Jasenek, and H.-W. Schock, *J. Phys. Chem.* **B**(104), 4849 (2000).
15. U. Rau and H. W. Schock, *Appl. Phys. A: Mater. Sci. Process.* **69**, 131 (1999).
16. A. Rockett and R. W. Birkmire, *J. Appl. Phys.* **70**, R81 (1991).
17. B. J. Stanbery, *Crit. Rev. Solid State Mater. Sci.* **27**, 73 (2002).
18. H.-W. Schock and R. Noufi, *Prog. Photovolt.: Res. Appl.* **8**, 151 (2000).
19. S. Siebentritt, *Thin Solid Films* **403–404**, 1 (2002).
20. ASTM E927-91. Standard specification for solar simulation for terrestrial photovoltaic testing.
21. ASTM G159-98. Standard tables for references solar spectral irradiance at air mass 1.5: Direct normal and hemispherical for a 37 tilted surface (E891 & E892).
22. D. M. Chapin, C. S. Fuller, and G. L. Pearson, *J. Appl. Phys.* **25**, 676 (1954).
23. M. A. Green, K. Emery, D. L. King, S. Igari, and W. Warta, *Prog. Photovolt: Res. Appl.* **11**, 347 (2003).
24. T. Kojima, T. Koyanagi, K. Nakamura, T. Yanagisawa, K. Takahisa, M. Nishitani, and T. Wada, *Sol. Energy Mater. Sol. Cells* **50**, 87 (1998).
25. V. M. Fthenakis, S. C. Morris, P. D. Moskowitz, and D. L. Morgan, *Prog. Photovolt.: Res. Appl.* **7**, 489 (1999) and references cited therein.
26. T. Wada, N. Kohara, S. Nishiwaki, and T. Negami, *Thin Solid Films* **387**, 118 (2001).
27. D. Schmid, M. Ruckh, and H. W. Schock, *Sol. Energy Mater. Sol. Cells* **41/42**, 281 (1996).
28. H. W. Schock and U. Rau, *Physica B* **308–310**, 1081 (2001).
29. J. -F. Guillemoles, P. Cowache, A. Lusson, K. Fezzaa, F. Boisivon, J. Vedel, and D. Lincot, *J. Appl. Phys.* **79**, 7293 (1996).

30. R. J. Schwartz and J. L. Gray, *Conf. Rec. 21st IEEE Photovolt. Spec. Conf.*, IEEE, New York, 570 (1990).
31. C. Heske, D. Eich, R. Fink, E. Umbach, T. van Buuren, C. Bostedt, L. J. Terminello, S. Kakar, M. M. Grush, T. A. Callcott, F. J. Himpsel, D. L. Ederer, R. C. C. Perera, W. Riedl, and F. Karg, *Appl. Phys. Lett.* **74**, 1451 (1999).
32. T. Nakada and A. Kunioka, *Appl. Phys. Lett.* **74**, 2444 (1999).
33. T. Nakada, T. Kume, T. Mise, and A. Kunioka, *Jpn. J. Appl. Phys.* **37**, L499 (1998).
34. F.-J. Haug, D. Rudmann, G. Bilger, H. Zogg, and A. N. Tiwari, *Thin Solid Films* **403–404**, 293 (2002).
35. F.-J. Haug, D. Rudmann, H. Zogg, A. N. Tiwari, *Thin Solid Films* **431–432**, 431 (2003).
36. Powder Diffraction Files, Card 40–1487, International Centre for Diffraction Data, Newtown Square, Pennsylvania, PA.
37. J. M. Merino, J. L. Martín de Vidales, S. Mahanty, R. Díaz, F. Rueda, and M. León, *J. Appl. Phys.* **80**, 5610 (1996).
38. Powder Diffraction Files, Card 23-0207, International Centre for Diffraction Data, Newtown Square, Pennsylvania, PA.
39. D. Schmid, M. Ruckh, F. Grunwald, and H. W. Schock, *J. Appl. Phys.* **73**, 2902 (1993).
40. I. M. Kötschau and H. W. Schock, *J. Phys. Chem. Solids* **64**, 1559 (2003).
41. B. Canawa, J. F. Guillemoles, J. Vigneron, D. Lincot, and A. Etcheberry, *J. Phys. Chem. Solids* **64**, 1791 (2003).
42. R. Klenk, *Thin Solid Films* **387**, 135 (2001).
43. S. H. Kwon, S. C. Park, B. T. Ahn, K. H. Yoon, and J. Song, *Sol. Energy* **64**, 55 (1998).
44. T. Negami, N. Kohara, M. Nishitani, T. Wada, and T. Hirao, *Appl. Phys. Lett.* **67**, 825 (1995).
45. S. B. Zhang, S.-H. Wei, A. Zunger, and H. Katayama-Yoshida, *Phys. Rev. B* **57**, 9642 (1998).
46. J. A. M. AbuShama, S. Johnston, T. Moriarty, G. Teeter, K. Ramanathan, and R. Noufi, *Prog. Photovolt: Res. Appl.* **12**, 39 (2004).
47. D. L. Young, J. Keane, A. Duda, J. A. M. AbuShama, C. L. Perkins, M. Romero, and R. Noufi, *Prog. Photovolt: Res. Appl.* **11**, 535 (2003).
48. J. Klaer, J. Bruns, R. Henninger, K. Siemer, R. Klenk, K. Ellmer, and D. Bräunig, *Semicond. Sci. Technol.* **13**, 1456 (1998).
49. M. A. Contreras, B. Egaas, K. Ramanathan, J. Hiltner, A. Swartzlander, F. Hasoon, and R. Noufi, *Prog. Photovolt.: Res. Appl.* **7**, 311 (1999).
50. T. Negami, Y. Hashimoto, and S. Nishiwaki, *Sol. Energy Mater. Sol. Cells* **67**, 331 (2001).
51. Y. Hagiwara, T. Nakada, and A. Kunioka, *Sol. Energy Mater. Sol. Cells* **67**, 267 (2001).
52. S. Chaisitsak, A. Yamada, and M. Konagai, *Jpn. J. Appl. Phys.* **41**, 507 (2002).
53. T. Nakada, and M. Mizutani, *Jpn. J. Appl. Phys.* **41**, L165 (2002).
54. S. B. Zhang, S.-H. Wei, and A. Zunger, *J. Appl. Phys.* **83**, 3192 (1998).
55. M. Turcu, O. Pakma, and U. Rau, *Appl. Phys. Lett.* **80**, 2598 (2002).
56. M. Turcu, and U. Rau, *J. Phys. Chem. Solids* **64**, 1591 (2003).
57. M. Turcu, and U. Rau, *Thin Solid Films* **431–432**, 158 (2003).
58. U. Rau, A. Jasenek, H. W. Schock, F. Engelhardt, and Th. Meyer, *Thin Solid Films* **361–362**, 298 (2000).
59. U. Rau, M. Schmidt, A. Jasenek, G. Hanna, and H. W. Schock, *Sol. Energy Mater. Sol. Cells* **67**, 137 (2001).
60. W. N. Shafarman, R. Klenk, and B. E. McCandless, *J. Appl. Phys.* **79**, 7324 (1996).
61. G. Hanna, A. Jasenek, U. Rau, and H. W. Schock, *Thin Solid Films* **387**, 71 (2001).
62. M. A. Contreras, J. Tuttle, A. Gabor, A. Tennant, K. Ramanathan, S. Asher, A. Franz, J. Keane, L. Wang, J. Scofield, and R. Noufi, *Proc. 1st World Conf. Photovolt. Energy Conv.*, IEEE, Piscataway, NJ., 68 (1994).
63. T. Dullweber, O. Lundberg, J. Malmström, M. Bodegård, L. Stolt, U. Rau, H. W. Schock, and J. H. Werner, *Thin Solid Films* **387**, 11 (2001).
64. O. Lundberg, M. Bodegård, J. Malmström, and L. Stolt, *Prog. Photovolt: Res. Appl.* **11**, 77 (2003).
65. T. Dullweber, G. Hanna, W. Shams-Kolahi, A. Schwartzlander, M. A. Contreras, R. Noufi, and H. W. Schock, *Thin Solid Films* **361–362**, 478 (2000).
66. J. Tringe, J. Nocerino, R. Tallon, W. Kemp, W. Shafarman, and D. Marvin, *J. Appl. Phys.* **91**, 516 (2002).
67. A. Jasenek, U. Rau, K. Weinert, I. M. Kötschau, G. Hanna, G. Voorwinden, M. Powalla, H. W. Schock, and J. H. Werner, *Thin Solid Films* **387**, 228 (2001).
68. A. Jasenek and U. Rau, *J. Appl. Phys.* **90**, 650 (2001).
69. M. Yamaguchi, *J. Appl. Phys.* **78**, 1476 (1995).
70. S. Kawakita, M. Imaizumi, M. Yamaguchi, K. Kushiya, T. Ohshima, H. Itoh, and S. Matsuda, *Jpn. J. Appl. Phys., Part 2* **41**, L797 (2002).
71. A. Boden, D. Bräunig, J. Klaer, F. H. Karg, B. Hosselbarth, and G. La Roche, *Conf. Rec. 28th IEEE Photovolt. Spec. Conf.*, IEEE, Piscataway, N.J., 1038 (2000).
72. S. H. Wei, S. B. Zhang, and A. Zunger, *Appl. Phys. Lett.* **72**, 3199 (1998).
73. P. Zabierowski, U. Rau, and M. Igalson, *Thin Solid Films* **387**, 147 (2001).
74. M. Köntges, R. Reineke-Koch, P. Nollet, J. Beier, R. Schäffler, and J. Parisi, *Thin Solid Films* **403–404**, 280 (2002).
75. J.-F. Guillemoles, U. Rau, L. Kronik, H.-W. Schock, and D. Cahen, *Adv. Mater.* **11**, 957 (1999).
76. J. Hedström, H. Ohlsen, M. Bodegård, A. Kylner, L. Stolt, D. Hariskos, M. Ruckh, and H.-W. Schock, *Conf. Rec. 23rd IEEE Photovolt. Spec. Conf.* IEEE, Piscataway, N.J., 364 (1993).
77. L. Stolt, J. Hedström, J. Kessler, M. Ruckh, K.-O. Velthaus, and H.-W. Schock, *Appl. Phys. Lett.* **62**, 597 (1993).
78. K. Granath, M. Bodegård, and L. Stolt, *Sol. Energy Mater. Sol. Cells* **60**, 279 (2000).
79. M. Bodegård, K. Granath, and L. Stolt, *Thin Solid Films* **361–362**, 9 (2000).
80. D. Rudmann, G. Bilger, M. Kaelin, F.-J. Haug, H. Zogg, and A. N. Tiwari, *Thin Solid Films* **431–432**, 37 (2003).
81. M. Lammer, U. Klemm, and M. Powalla, *Thin Solid Films* **387**, 33 (2001).
82. M. A. Contreras, B. Egaas, P. Dippo, J. Webb, J. Granata, K. Ramanathan, S. Asher, A. Swartzlander, and R. Noufi, *Conf. Rec. 26th IEEE Photovolt. Spec. Conf.*, IEEE, Piscataway, N.J., 359 (1997).
83. B. M. Keyes, F. Hasoon, P. Dippo, A. Balcioglu, and F. Abulfotuh, *Conf. Rec. 26th IEEE Photovolt. Spec. Conf.*, IEEE, Piscataway, N.J., 479, 1997.

84. T. Nakada, D. Iga, H. Ohbo, and A. Kunioka, *Jpn. J. Appl. Phys.* **36** , 732 (1997).
85. J. E. Granata, J. R. Sites, S. Asher, and J. Matson, *Conf. Rec. 26th IEEE Photovolt. Spec. Conf.*, IEEE, Piscataway, N. J., 387 (1997).
86. G. Hanna, J. Mattheis, V. Laptev, Y. Yamamoto, U. Rau, and H. W. Schock, *Thin Solid Films* **431–432**, 31 (2003).
87. O. Lundberg, J. Lu, A. Rockett, M. Edoff, and L. Stolt, *J. Phys. Chem. Solids* **64**, 1499 (2003).
88. D. Braunger, D. Hariskos, G. Bilger, U. Rau, H. W. Schock, *Thin Solid Films* **361–362**, 161 (2000).
89. C. Heske, D. Eich, R. Fink, E. Umbach, S. Kakar, T. van Buuren, C. Bostedt, L. J. Terminello, M. M. Grush, T. A. Callcott, F. J. Himpsel, D. L. Ederer, R. C. C. Perera, W. Riedl, and F. Karg, *Appl. Phys. Lett.* **75**, 2082 (1999).
90. D. W. Niles, K. Ramanathan, F. Hasoon, R. Noufi, B. J. Tielsch, and J. E. Fulghum, *J. Vac. Sci. Technol. A* **15**, 3044 (1997).
91. A. Rockett, J. S. Britt, T. Gillespie, C. Marshall, M. M. Al Jassim, F. Hasoon, R. Matson, and B. Başol, *Thin Solid Films* **372**, 212 (2000).
92. R. Kimura, T. Nakada, P. Fons, A. Yamada, S. Niki, T. Matsuzawa, K. Takahashi, and A. Kunioka, *Sol. Energy Mater. Sol. Cells* **67**, 289 (2001).
93. S.-H. Wei, S. B. Zhang, and A. Zunger, *J. Appl. Phys.* **85**, 7214 (1999).
94. A. Rockett, K. Granath, S. Asher, M. M. Al Jassim, F. Hasoon, R. Matson, B. Başol, V. Kapur, J. S. Britt, T. Gillespie, and C. Marshall, *Sol. Energy Mater. Sol. Cells.* **59**, 255 (1999).
95. M. Ruckh, D. Scmid, M. Kaiser, R. Schäffler, T. Walter, and H. W. Schock, *Proc. 1st World Conf. Photovolt. Energy Conv.*, IEEE; Piscataway, N.J., 156 (1994).
96. P. F. Gerhardinger and R. J. McCurdy, *Mater. Res. Soc. Symp. Proc.* **426**, 399 (1996).
97. A. Mills, A. Lepre, N. Elliott, S. Bhopal, I. P. Parkin, and S. A. O'Neill, *J. Photochem. Photobiol. A: Chem.* **160**, 213 (2003).
98. L. Kronik, D. Cahen, and H. W. Schock, *Adv. Mater.* **10**, 31 (1998).
99. D. Cahen and R. Noufi, *Appl. Phys. Lett.* **54**, 558 (1989).
100. L. Kronik, U. Rau, J.-F. Guillemoles, D. Braunger, H. W. Schock, and D. Cahen, *Thin Solid Films* **361–362**, 353 (2000).
101. U. Rau, D. Braunger, R. Herberholz, H. W. Schock, J.-F. Guillemoles, L. Kronik, and D. Cahen, *J. Appl. Phys.* **86**, 497 (1999).
102. M. B. Zellner, R. W. Birkmire, E. Eser, W. N. Shafarman, and J. G. Chen, *Prog. Photovolt: Res. Appl.* **11**, 543 (2003).
103. R. Caballero and C. Guillén, *Thin Solid Films* **403–404**, 107 (2002).
104. M. Marudachalam, H. Hichri, R. Klenk, R. W. Birkmire, W. N. Shafarman, and J. M. Schultz, *Appl. Phys. Lett.* **67**, 3978 (1995).
105. M. Klenk, O. Schenker, V. Alberts, and E. Bucher, *Semicond. Sci. Technol.* **17**, 435 (2002).
106. W. E. Devaney, W. S. Chen, J. M. Stewart, and R. A. Mickelsen, *IEEE Trans. Electron Dev.* **37**, 428 (1990).
107. A. M. Gabor, J. R. Tuttle, D. S. Albin, M. A. Contreras, and R. Noufi, *Appl. Phys. Lett.* **65**, 198 (1994).
108. J. Kessler, C. Chityuttakan, J. Lu, J. Schöldström, and L. Stolt, *Prog. Photovolt: Res. Appl.* **11**, 319 (2003).
109. O. Lundberg, M. Bodegård, and L. Stolt, *Thin Solid Films* **431–432**, 26 (2003).
110. W. N. Shafarman, and J. Zhu, *Thin Solid Films* **361–362**, 473 (2000).
111. M. A. Contreras, B. Egaas, D. King, A. Schwartzlander, and T. Dullweber, *Thin Solid Films* **361–362**, 167 (2000).
112. M. A. Contreras, K. M. Jones, L. Gedvilas, and R. Matson, *Proc. 16th Eur. Photovolt. Solar Energy Conf.*, James & James, London, 732 (2001).
113. A. M. Hermann, C. Gonzalez, P. A. Ramakrishnan, D. Balzar, N. Popa, B. Rice, C. H. Marshall, J. N. Hilfiker, T. Tiwald, P. J. Sebastian, M. E. Calixto, and R. N. Bhattacharya, *Sol. Energy Mater. Sol. Cells* **70**, 345 (2001).
114. T. Negami, T. Satoh, Y. Hashimoto, S. Shimakawa, S. Hayashi, M. Muro, H. Inoue, and M. Kitagawa, *Thin Solid Films* **403–404**, 197 (2002).
115. M. Powalla and B. Dimmler, *Thin Solid Films* **361–362**, 540 (2000).
116. B. Dimmler, E. Gross, R. Menner, M. Powalla, D. Hariskos, M. Ruckh, U. Rühle, and H. W. Schock, *Conf. Rec. 25th IEEE Photovolt. Spec. Conf.* IEEE, Piscataway, 757 (1996).
117. K. Knapp, and T. Jester, *Sol. Energy* **71**, 165 (2001).
118. J. Zank, M. Mehlin, and H. P. Fritz, *Thin Solid Films* **286**, 259 (1996).
119. K. T. Ramakrishna Reddy, P. K. Datta, and M. J. Carter, *Phys. Stat. Sol. (a)* **182**, 679 (2000).
120. F. O. Adurodija, J. Song, S. D. Kim, S. H. Kwon, S. K. Kim, K. H. Yoon, and B. T. Ahn, *Thin Solid Films* **338**, 13 (1999).
121. M. Marudachalam, R. W. Birkmire, H. Hichri, J. M. Schultz, A. Swartzlander, and M. M. Al-Jassim, *J. Appl. Phys.* **82**, 2896 (1997).
122. C. Guillén, M. A. Martínez, and J. Herrero, *Vacuum* **58**, 594 (2000).
123. Ö. F. Yüksel, B. M. Başol, H. Safak, and H. Karabiyik, *Appl. Phys. A* **73**, 387 (2001).
124. A. G. Chowles, J. H. Neethling, H. van Niekerk, J. A. A. Engelbrecht, and V. J. Watters, *Renew. Energy* **6** 613 (1995).
125. S. Bandyopadhyaya, S. Roy, S. Chaudhuri, and A. K. Pal, *Vacuum* **62**, 61 (2001).
126. C. Guillén and J. Herrero, *Sol. Energy Mater. Sol. Cells* **73**, 141 (2002).
127. M. S. Sadigov, M. Özkan, E. Bakacsiz, M. Altunbaş, and A. I. Kopya, *J. Mater. Sci.* **34**, 4579 (1999).
128. T. L. Chu, S. S. Chu, S. C. Lin, and J. Yue, *J. Electrochem. Soc.* **131**, 2182 (1984).
129. J. Bekker, V. Alberts, and M. J. Witcomb, *Thin Solid Films* **387**, 40 (2001).
130. S. F. Chichibu, M. Sugiyama, M. Ohbasami, A. Hayakawa, T. Mizutani, H. Nakanishi, T. Negami, and T. Wada, *J. Cryst. Growth* **243**, 404 (2002).
131. A. Garg, K. S. Balakrisnan, and A. C. Rastogi, *J. Electrochem. Soc.* **141**, 1566 (1994).
132. A. C. Rastogi, K. S. Balakrisnan, R. K. Sharma, and K. Jain, *Thin Solid Films,* **357**, 179, 1999.
133. C. Guillén, and J. Herrero, *Thin Solid Films* **323**, 93 (1998).
134. V. Alberts, M. Klenk, and E. Bucher, *Thin Solid Films* **387**, 44 (2001).
135. M. E. Calixto, and P. J. Sebastian, *J. Mater. Sci*. **33**, 339 (1998).
136. G. Hodes, T. Engelhardt, D. Cahen, L. L. Kazmerski, and C. R. Herrington, *Thin Solid Films* **128**, 93 (1985).

137. S. R. Kumar, R. B. Gore, and R. K. Pandey, *Thin Solid Films* **223**, 109 (1993).
138. H. P. Fritz and P. Chatziagorastou, *Thin Solid Films* **247**, 129 (1994).
139. V. K. Kapur, B. M. Başol, and E. S. Tseng, *Sol. Cells* **21**, 65 (1987).
140. P. P. Prosini, M. L. Addonizio, A. Antonaia and S. Loreti, *Thin Solid Films* **288**, 90 (1996).
141. M. Altosaar, E. Mellikov, J. Kois, Y. Guo, and D. Meissner, *Proceedings of Joint International Meeting of The Electrochemical Society, Inc. and The International Society of Electrochemistry* Paris, France, 1314 (1997).
142. C. D. Lokhande, *Bull. Electrochem.* **4**, 131 (1988).
143. L. X. Shao, K. H. Chang, T. H. Chung, B. H. Tseng, and H. L. Hwang, *J. Phys. Chem. Solids* **64**, 1505 (2003).
144. J. Bekker, V. Alberts, A. W. R. Leitch, and J. R. Botha, *Thin Solid Films* **431–432**, 116 (2003).
145. P. Berwian, A. Weimar, and G. Müller, *Thin Solid Films* **431–432**, 41 (2003).
146. V. Probst, W. Stetter, W. Riedl, H. Vogt, M. Wendl, H. Calwer, S. Zweigart, K.-D. Ufert, B. Freienstein, H. Cerva, and F. Karg, *Thin Solid Films* **387**, 262 (2001).
147. B. M. Başol, A. Halani, C. Leidholm, G. Norsworthy, V. K. Kapur, A. Swartzlander, and R. Matson, *Prog. Photovolt.: Res. Appl.* **8**, 227 (2000).
148. J. Keränen, J. Lu, J. Barnard, J. Sterner, J. Kessler, L. Stolt, Th. W. Matthes, and E. Olsson, *Thin Solid Films* **387**, 80 (2001).
149. T. Wada, Y. Hashimoto, S. Nishiwaki, T. Satoh, S. Hayashi, T. Negami, and H. Miyake, *Sol. Energy Mater. Sol. Cells* **67**, 305 (2001).
150. K. Kushiya, M. Tachiyuki, Y. Nagoya, A. Fujimaki, B. Sang, D. Okumura, M. Satoh, and O. Yamase, *Sol. Energy Mater. Sol. Cells* **67**, 11 (2001).
151. K. Kushiya, *Thin Solid Films* **387**, 257 (2001).
152. F. H. Karg, *Sol. Energy Mater. Sol. Cells* **66**, 645 (2001).
153. T. J. Gillespie, C. H. Marshall, M. Contreras, and J. Keane, *Sol. Energy Mater. Sol. Cells* **59**, 27 (1999).
154. A. M. Hermann, M. Mansour, V. Badri, B. Pinkhasov, C. Gonzales, F. Fickett, M. E. Calixto, P. J. Sebastian, C. H. Marshall, and T. J. Gillespie, *Thin Solid Films* **361–362**, 74 (2000).
155. A. M. Hermann, C. Gonzalez, P. A. Ramakrishnan, D. Balzar, C. H. Marshall, J. N. Hilfiker, and T. Tiwald, *Thin Solid Films* **387**, 54 (2001).
156. S. C. Park, D. Y. Lee, B. T. Ahn, K. H. Yoon, and J. Song, *Sol. Energy Mater. Sol. Cells* **69**, 99 (2001).
157. D. Y. Lee, J. H. Yun, B. T. Ahn, K. H. Yoon, and J. Song, *Mater. Res. Soc. Symp. Proc.* **668**, H8.8.1-6 (2001).
158. A. Ashida, Y. Hachiuma, N. Yamamoto, T. Ito, and Y. Cho, *J. Mater. Sci. Lett.,* **13**, 1181, 1994.
159. T. Yamaguchi, T. Naoyama, H. S. Lee, A. Yoshida, T. Kobata, S. Niiyama, and T. Nakamura, *J. Phys. Chem. Solids* **64**, 1831 (2003).
160. M. Klenk, O. Schenker, V. Alberts, and E. Bucher, *Thin Solid Films* **387**, 47 (2001).
161. J. M. Merino, M. León, F. Rueda, and R. Diaz, *Thin Solid Films* **361–362**, 22 (2000).
162. H. Sakata and H. Ogawa, *Sol. Energy Mater. Sol. Cells* **63**, 259 (2000).
163. A. A. S. Akl, A. Ashour, A. A. Ramadan, and K. A. El-Hady, *Vacuum* **61**, 75 (2001).
164. C. M. Joseph and C. S. Menon, *J. Phys. D: Appl. Phys.* **34**, 1143 (2001).
165. P. Victor, J. Nagaraju, and S. B. Krupanidhi, *Solid State Comm.* **116**, 649 (2000).
166. S. Kuranouchi and A. Yoshida, *Thin Solid Films* **343–344**, 123 (1999).
167. S. Duchemin, M. C. Artaud, F. Ouchen, and J. Bougnot, *J. Mater. Sci.: Mater. Electron.* **7**, 201 (1996).
168. M. C. Artaud, F. Ouchen, L. Martin, and S. Duchemin, *Thin Solid Films* **324**, 115 (1998).
169. P. A. Jones, A. D. Jackson, P. D. Lickiss, R. D. Pilkington, and R. D. Tomlinson, *Thin Solid Films* **238**, 4 (1994).
170. J. McAleese, P. O'Brien, and D. J. Otway, *Chem. Vap. Deposition* **4**, 94 (1998).
171. J.-H. Park, M. Afzaal, M. Kemmler, P. O'Brien, D. J. Otway, J. Raftery, and J. Waters, *J. Mater. Chem.* **13**, 1942 (2003).
172. M. Afzaal, D. J. Crouch, P. O'Brien, J. Raftery, P. J. Skabara, A. J. P. White, and D. J. Williams, *J. Mater. Chem.* **14**, 233 (2004).
173. K. K. Banger, M. H.-C. Jin, J. D. Harris, P. E. Fanwick, and A. F. Hepp, *Inorg. Chem.* **42**, 7713 (2003).
174. J. A. Hollingsworth, K. K. Banger, M. H.-C. Jin, J. D. Harris, J. E. Cowen, E. W. Bohannan, J. A. Switzer, W. E. Buhro, and A. F. Hepp, *Thin Solid Films*, **431–432**, 63 (2003).
175. G. W. El Haj Moussa, Ariswan, A. Khoury, F. Guastavino, and C. Llinarés, *Solid State Comm.* **122**, 195 (2002).
176. G. Massé, K. Djessas, C. Monty, and F. Sibieude, *Thin Solid Films* **414**, 192 (2002).
177. K. T. R. Reddy, and R. W. Miles, *J. Mater. Sci.: Mater. Electron.* **14**, 529 (2003).
178. S. Shirakata, Y. Kannaka, H. Hasegawa, T. Kariya, and S. Isomura, *Jpn. J. Appl. Phys.* **38**, 4997 (1999).
179. R. N. Bhattacharya, *J. Electrochem. Soc.* **130**, 2040 (1983).
180. L. Thouin, S. Massaccesi, S. Sanchez, and J. Vedel, *J. Electroanal. Chem.* **374**, 81 (1994).
181. T. Pottier and G. Maurin, *J. Appl. Electrochem.* **19**, 361 (1989).
182. A. N. Molin, A. I. Dikusar, G. A. Kiosse, P. A. Petrenko, A. I. Sokolovsky, and Yu. G. Saltanovsky, *Thin Solid Films* **237**, 66 (1994).
183. A. N. Molin and A. I. Dikusar, *Thin Solid Films* **237**, 72 (1994).
184. M. G. Ganchev and K. D. Kochev, *Sol. Energy Mater. Sol. Cells* **31**, 163 (1993).
185. Guillén, C., and J. Herrero, *J. Electrochem. Soc.* **141**, 225 (1994).
186. Y. Ueno, H. Kawai, T. Sugiura, and H. Minoura, *Thin Solid Films* **157**, 159 (1988).
187. R. P. Raffaelle, H. Forsell, T. Potdevin, R. Friedfeld, J. G. Mantovani, S. G. Bailey, S. M. Hubbard, E. M. Gordon, and A. F. Hepp, *Sol. Energy Mater. Sol. Cells.* **57**, 167 (1999).
188. E. Tzvetkova, N. Stratieva, M. Ganchev, I. Tomov, K. Ivanova, and K. Kochev, *Thin Solid Films* **311**, 101 (1997).
189. T. Edamura, and J. Muto, *J. Mater. Sci.* **5**, 275 (1994).
190. A. Kampmann, V. Sittinger, J. Rechid, and R. Reineke-Koch, *Thin Solid Films* **361–362**, 309 (2000).
191. N. B. Chaure, J. Young, A. P. Samantilleke, and I. M. Dharmadasa, *Sol. Energy Mater. Sol. Cells*, **81**, 125 (2004).
192. R. N. Bhattacharya, J. F. Hiltner, W. Batchelor, M. A. Contreras, R. N. Noufi, and J. R. Sites, *Thin Solid Films* **361–362**, 396 (2000).

193. R. N. Bhattacharya, W. Batchelor, K. Ramanathan, M. A. Contreras, and T. Moriarty, *Sol. Energy Mater. Sol. Cells* **63**, 367 (2000).
194. P. Garg, A. Garg, A. C. Rastogi, and J. C. Garg, *J. Phys. D: Appl. Phys.* **24**, 2026 (1991).
195. S. N. Sahu, R.D. L. Kristensen, and D. Haneman, *Sol. Energy Mater.* **18**, 385 (1989).
196. Y. Sudo, S. Endo, and T. Irie, *Jpn. J. Appl. Phys.* **32**, 1562 (1993).
197. M. C. F. Oliveira, M. Azevedo, and A. Cunha, *Thin Solid Films* **405**, 129 (2002).
198. M. E. Calixto and P. J. Sebastian, *Sol. Energy Mater. Sol. Cells* **63**, 335 (2000).
199. R. Ugarte, R. Schrebler, R. Córdova, E. A. Dalchiele, and H. Gómez, *Thin Solid Films* **340**, 117 (1999).
200. C. D. Lokhande, *J. Electrochem. Soc.* **134**, 1727 (1987).
201. S. Nomura, K. Nishiyama, K. Tanaka, M. Sakakibara, M. Ohtsubo, N. Furutani, and S. Endo, *Jpn. J. Appl. Phys.* **37**, 3232 (1998).
202. S. N. Qiu, L. Li, C. X. Qiu, I. Shih, and C. H. Champness, *Sol. Energy Mater. Sol. Cells* **37**, 389 (1995).
203. M. Pourbaix, *Atlas of Electrochemical Equilibria in Aqueous Solutions*, Pergamon Press, New York, 1966.
204. F. Chraibi, M. Fahoume, A. Ennaoui, and J. L. Delplancke, *Phys. Stat. Sol. (a)* **186**, 373 (2001).
205. F. J. Pern, R. Noufi, A. Mason, and A. Franz, *Thin Solid Films* **202**, 299 (1991).
206. M. Kemell, M. Ritala, H. Saloniemi, M. Leskelä, T. Sajavaara, and E. Rauhala, *J. Electrochem. Soc.* **147**, 1080 (2000).
207. M. Kemell, M. Ritala, and M. Leskelä, *J. Mater. Chem.* **11**, 668 (2001).
208. L. Zhang, F. D. Jiang, and J. Y. Feng, *Sol. Energy Mater. Sol. Cells* **81**, 483 (2004).
209. L. Thouin and J. Vedel, *J. Electrochem. Soc.* **142**, 2996 (1995).
210. F. A. Kröger, *J. Electrochem. Soc.* **125**, 2028 (1978).
211. M. P. R. Panicker, M. Knaster, and F. A. Kröger, *J. Electrochem. Soc.* **125**, 566 (1978).
212. R. K. Pandey, S. N. Sahu, and S. Chandra, *Handbook of Semiconductor Electrodeposition*, Marcel Dekker, New York, 1996.
213. H. Saloniemi, T. Kanniainen, M. Ritala, and M. Leskelä, *Thin Solid Films* **326**, 78 (1998).
214. H. Saloniemi, T. Kanniainen, M. Ritala, M. Leskelä, and R. Lappalainen, *J. Mater. Chem.* **8**, 651 (1998).
215. S. Massaccesi, S. Sanchez, and J. Vedel, *J. Electrochem. Soc.* **140**, 2540 (1993).
216. M. Kemell, H. Saloniemi, M. Ritala, and M. Leskelä, *Electrochim. Acta*, **45**, 3737 (2000).
217. S. Ahrland, and B. Tagesson, *Acta Chem. Scand. A* **31**, 615 (1977).
218. R. M. Smith, and A. E. Martell, *NIST Critically Selected Stability Constants for Metal Complexes Database* Version 4.0, (1997).
219. M. Kemell, H. Saloniemi, M. Ritala, and M. Leskelä, *J. Electrochem. Soc.* **148**, C110 (2001).
220. S. N. Qiu, W. W. Lam, C. X. Qiu, and I. Shih, *Appl. Surf. Sci.* **113/114**, 764 (1997).
221. C. X. Qiu, and I. Shih, *Can. J. Phys.* **65**, 1011 (1987).
222. M. Kemell, *Electrodeposition of $CuInSe_2$ and doped ZnO thin films for solar cells*, Ph.D. Thesis, University of Helsinki, 2003.
223. M. Kemell, F. Dartigues, M. Ritala, and M. Leskelä, *Thin Solid Films* **434**, 20 (2003).
224. R. N. Bhattacharya, W. Batchelor, J. E. Granata, F. Hasoon, H. Wiesner, K. Ramanathan, J. Keane, and R. N. Noufi, *Sol. Energy Mater. Sol. Cells*, **55**, 83 (1998).
225. D. Lincot, M. Froment, and H. Cachet, in *Advances in Electrochemical Science and Engineering*, **Vol. 6**, R. C. Alkire, D. M. Kolb, Eds., Wiley-VCH, Weinheim, Germany, 1999, 165.
226. J. C. Garg, R. P. Sharma, and K. C. Sharma, *Thin Solid Films* **164**, 269 (1988).
227. B. M. Başol, *Thin Solid Films* **361–362**, 514 (2000).
228. C. Eberspacher, C. Fredric, K. Pauls, and J. Serra, *Thin Solid Films* **387**, 18 (2001).
229. G. Norsworthy, C. R. Leidholm, A. Halani, V. K. Kapur, R. Roe, B. M. Başol, and R. Matson, *Sol. Energy Mater Sol. Cells* **60**, 127 (2000).
230. V. Kapur, A. Bansal, P. Le, and O. I. Asensio, *Thin Solid Films* **431–432**, 53 (2003).
231. M. Kaelin, D. Rudmann, F. Kurdesau, T. Meyer, H. Zogg, and A. N. Tiwari, *Thin Solid Films* **431–432**, 58 (2003).
232. U. Rau and M. Scmidt, *Thin Solid Films* **387**, 141 (2001).
233. M. A. Contreras, M. J. Romero, B. To, F. Hasoon, R. Noufi, S. Ward, and K. Ramanathan, *Thin Solid Films* **403–404**, 204 (2002).
234. Y. Hashimoto, N. Kohara, T. Negami, N. Nishitani, and T. Wada, *Sol. Energy Mater. Sol. Cells* **50**, 71 (1998).
235. A. Kylner, A. Rockett, and L. Stolt, *Solid State Phenom.* **51–52**, 533 (1996).
236. C. Guillén, M. A. Martínez, C. Maffiotte, and J. Herrero, *J. Electrochem. Soc.* **148**, G602 (2001).
237. A. Kylner, *J. Appl. Phys.* **85**, 6858 (1999).
238. T. M. Friedlmeier, D. Braunger, D. Hariskos, M. Kaiser, H. N. Wanka, and H. W. Schock, *Conf. Rec. 25th IEEE Photovolt. Spec. Conf.* IEEE Piscataway, N.J., 845 (1996).
239. *CRC Handbook of Chemistry and Physics* 82nd Ed., Edited by D. R. Lide, CRC Inc., Press, Boca Raton, FL 2001–2002.
240. B. Canawa, J.-F. Guillemoles, E.-B. Yousfi, P. Cowache, H. Kerber, A. Loeffl, H.-W. Schock, M. Powalla, D. Hariskos, and D. Lincot, *Thin Solid Films* **361–362**, 187 (2000).
241. M. Bär, H.-J. Muffler, C.-H. Fischer, S. Zweigart, F. Karg, and M. C. Lux-Steiner, *Prog. Photovolt.: Res. Appl.* **10**, 173 (2002).
242. B. M. Başol, V. K. Kapur, G. Norsworthy, A. Halani, C. R. Leidholm, and R. Roe, *Electrochem. Solid-State Lett.* **1**, 252 (1998).
243. K. Kushiya, T. Nii, I. Sugiyama, Y. Sato, Y. Inamori, and H. Takeshita, *Jpn. J. Appl. Phys.* **35**, 4383 (1996).
244. A. Ennaoui, S. Siebentritt, M. Ch. Lux-Steiner, W. Riedl, and F. Karg, *Sol. Energy Mater. Sol. Cells* **67**, 31 (2001).
245. D. Hariskos, M. Ruckh, U. Rühle, T. Walter, H. W. Schock, J. Hedström, and L. Stolt, *Sol. Energy Mater. Sol. Cells* **41/42**, 345, 1996.
246. H.-J. Muffler, M. Bär, C.-H. Fischer, R. Gay, F. Karg, and M. C. Lux-Steiner, *Conf. Rec. 28th IEEE Photovolt. Spec. Conf.*, IEEE Piscataway, N.J., 610 (2000).
247. S. Siebentritt, T. Kampschulte, A. Bauknecht, U. Blieske, W. Harneit, U. Fiedeler, and M. Lux-Steiner, *Sol. Energy Mater. Sol. Cells* **70**, 447 (2002).
248. J.-F. Guillemoles, B. Canawa, E. B. Yousfi, P. Cowache, A. Galtayries, T. Asikainen, M. Powalla, D. Hariskos, H.-W. Schock, and D. Lincot, *Jpn. J. Appl. Phys.* **40**, 6065 (2001).

249. E. B. Yousfi, T. Asikainen, V. Pietu, P. Cowache, M. Powalla, and D. Lincot, *Thin Solid Films* **361–362**, 183 (2000).
250. Y. Ohtake, K. Kushiya, M. Ichikawa, A. Yamada, and M. Konagai, *Jpn. J. Appl. Phys.* **34**, 5949 (1995).
251. Y. Ohtake, T. Okamoto, A. Yamada, M. Konagai, and K. Saito, *Sol. Energy Mater. Sol. Cells* **49**, 269 (1997).
252. Y. Ohtake, M. Ichikawa, T. Okamoto, A. Yamada, M. Konagai, and K. Saito, *Conf. Rec. 25th IEEE Photovolt. Spec. Conf.*, IEEE Piscataway, N.J., 793, 1996.
253. J. R. Tuttle, T. A. Berens, J. Keane, K. R. Ramanathan, J. Granata, R. N. Bhattacharya, H. Wiesner, M. A. Contreras, and R. Noufi, *Conf. Rec. 25th IEEE Photovolt. Spec. Conf.*, Piscataway, N.J., IEEE, 797, 1996.
254. A. Delahoy, J. Bruns, L. Chen, M. Akhtar, Z. Kiss, and M. Contreras, *Conf. Rec. 28th IEEE Photovolt. Spec. Conf.* Piscataway IEEE, 1437, 2000.
255. T. Sugiyama, S. Chaisitsak, A. Yamada, M. Konagai, Y. Kudriavtsev, A. Godines, A. Villegas, and R. Asomoza, *Jpn. J. Appl. Phys.* **39**, 4816 (2000).
256. T. Nakada and M. Mizutani, *Conf. Rec. 28th IEEE Photovolt. Spec. Conf.* IEEE Piscataway, N.J., 529, 2000.
257. K. Kushiya and O. Yamase, *Jpn. J. Appl. Phys.* **39**, 2577 (2000).
258. D. Gal, G. Hodes, D. Lincot, and H.-W. Schock, *Thin Solid Films* **361–362**, 79 (2000).
259. D. Hariskos, M. Powalla, N. Chevaldonnet, D. Lincot, A. Schindler, and B. Dimmler, *Thin Solid Films* **387**, 179 (2001).
260. N. Naghavi, S. Spiering, M. Powalla, B. Cavana, and D. Lincot, *Prog. Photovolt: Res. Appl.* **11**, 437 (2003).
261. N. F. Cooray, K. Kushiya, A. Fujimaki, I. Sugiyama, T. Miura, D. Okumura, M. Sato, M. Ooshita, and O. Yamase, *Sol. Energy Mater. Sol. Cells* **49**, 291 (1997).
262. B. Sang, K. Kushiya, D. Okumura, and O. Yamase, *Sol. Energy Mater. Sol. Cells* **67**, 223 (2001).
263. S. Chaisitsak, T. Sugiyama, A. Yamada, and M. Konagai, *Jpn. J. Appl. Phys.* **38**, 4989 (1999).
264. L. Stolt, J. Hedström, and J. Skarp, *Proc. 1st World Conf. Photovolt. Energy Conv.* IEEE Piscataway, N.J., 250, 1994.
265. L. C. Olsen, F. W. Addis, L. Huang, W. N. Shafarman, P. Eschbach, and G. J. Exarhos, *Conf. Rec. 28th IEEE Photovolt. Spec. Conf.* IEEE, Piscataway, N.J., 458, 2000.